

MEASUREMENT OF BINARY PHASE EQUILIBRIA AND
TERNARY/QUATERNARY GAS ANTISOLVENT (GAS) SYSTEM
MEASUREMENT AND ANALYSIS

A Thesis
Presented to
The Academic Faculty

By
Donald Taylor, III

In Partial Fulfillment
Of the Requirements for the Degree
Master of Science in Chemical & Biomolecular Engineering
Georgia Institute of Technology

July 7, 2004

MEASUREMENT OF BINARY PHASE EQUILIBRIA AND
TERNARY/QUATERNARY GAS ANTISOLVENT (GAS) SYSTEM
MEASUREMENT AND ANALYSIS

Approved By:

Dr. Charles A. Eckert

Dr. Aryn Teja

Dr. Peter Ludovice

Date Approved: July 9, 2004

DEDICATION

This Thesis is dedicated to my late brother Darien L. Taylor.

ACKNOWLEDGEMENT

The author would like to thank everyone in his research group and in BGSA for all their support over the last two years and all the great friendships made. The author would especially like to acknowledge the assistance from Dr. David Bush and soon-to-be Dr. Michael Lazzaroni throughout the course of the research. The author is greatly appreciative to his advisor, Dr. Charles Eckert, who was very up front yet understanding during these two hectic years.

The author also wants to thank his family for being there the entire way, especially his father and grandfather for all their support and advice. The author is greatly appreciative of his girlfriend Aisha Stroman for the day to day support, and being there at the best of times and the worst of times.

The author gives credit and thanks to the financial support from the Erskine Love Foundation and the GEM Fellowship for funding his research and graduate education.

TABLE OF CONTENTS

Acknowledgments	i
Table of Contents	ii
List of Tables	iii
List of Figures	vi
Glossary (symbols and abbreviations)	xi
Summary	xv
Chapter 1: Introduction	1
Chapter 2: Literature Review	4
Chapter 3: The Paper	8
Introduction	8
Experimental Design	12
Theory	20
Results and Discussion	27
Conclusion	46
Chapter 4: Future Recommendations	47
Appendix A: Apparatus Assembly and Procedures	49
Appendix B: Experimental Data	64
Appendix C: Bubble Point Calculation Flow Chart	84
References	85

LIST OF TABLES

Table 3.1	Thermal properties of phenanthrene and acetaminophen	11
Table 3.2	Materials for the VLE experiments	12
Table 3.3	Materials for fractional crystallization experimentation	16
Table A-1:	Equipment	52
Table B-1:	Jerguson Cell Volume Calibration Values. Water volume height measured using an attached ruler on the Jerguson Cell with the fine measurement from the cathetometer	65
Table B-2:	Expansion Data of N-methyl-pyrrolidone at 40 °C	66
Table B-3:	Expansion data of Dichloromethane at 40 °C	66
Table B-4:	Expansion data for Acetone at 40 °C	67
Table B-5:	Expansion data for Tetrahydrofuran at 40 °C	67
Table B-6:	Expansion data for Nitromethane at 40 °C	68
Table B-7:	Expansion data for Acetonitrile at 40 °C	68
Table B-8:	CO ₂ (1) and Acetone (2) Binary mixture at 40 °C	70
Table B-9:	CO ₂ (1) and Nitromethane (2) Binary mixture at 40 °C	70
Table B-10:	CO ₂ (1) and Tetrahydrofuran (2) Binary mixture at 40 °C	71
Table B-11:	CO ₂ (1) and Dichloromethane (2) Binary mixture at 40 °C	71
Table B-12:	CO ₂ (1) and Acetonitrile (2) Binary mixture at 40 °C	72
Table B-13:	MOSCED Parameters for every component used in this thesis	72
Table B-14:	Experimental Mole fractions and pressures for Toluene/Phenanthrene/CO ₂ system at 25 °C	76
Table B-15:	PRSV-HV-UNIQUAC predicted concentrations for Toluene/Phenanthrene/CO ₂ system at 25 °C	76

Table B-16:	UNIQUAC interaction parameter matrix Toluene/Phenanthrene/CO ₂	76
Table B-17:	Experimental Mole fractions and pressures for Tetrahydrofuran/Phenanthrene/CO ₂ system at 25 °C	77
Table B-18:	PRSV-HV-UNIQUAC predicted concentrations for Tetrahydrofuran/Phenanthrene/CO ₂ system at 25 °C	77
Table B-19:	UNIQUAC interaction parameter matrix for Tetrahydrofuran/Phenanthrene/CO ₂	77
Table B-20:	Experimental Mole fractions and pressures for Acetone/Phenanthrene/CO ₂ system at 25 °C	78
Table B-21:	PRSV-HV-UNIQUAC predicted concentrations for Acetone/Phenanthrene/CO ₂ system at 25 °C	78
Table B-22:	UNIQUAC interaction parameter matrix for Acetone/Phenanthrene/CO ₂	78
Table B-23:	Experimental Mole fractions and pressures for Acetone/Acetaminophen/CO ₂ system at 25 °C	79
Table B-24:	PRSV-HV-UNIQUAC predicted concentrations for Acetone/Acetaminophen/CO ₂ system at 25 °C	79
Table B-25:	UNIQUAC interaction parameter matrix for Acetone/Acetaminophen/CO ₂	80
Table B-26:	Experimental Mole fractions and pressures for Ethanol/Acetaminophen/CO ₂ system at 25 °C	80
Table B-27:	PRSV-HV-UNIQUAC predicted concentrations for Ethanol/Acetaminophen/CO ₂ system at 25 °C	80
Table B-28:	UNIQUAC interaction parameter matrix for Ethanol/Acetaminophen/CO ₂	81
Table B-29:	Experimental Mole fractions and pressures for Toluene/Acetaminophen/Phenanthrene/CO ₂ system at 25 °C	81

Table B-30:	PRSV-HV-UNIQUAC predicted concentrations for Toluene/Acetaminophen/Phenanthrene/CO ₂ system at 25 °C	82
Table B-31:	UNIQUAC interaction parameter matrix for Toluene/Acetaminophen/Phenanthrene/CO ₂	82
Table B-32:	Experimental Mole fractions and pressures for Acetone/Acetaminophen/Phenanthrene/CO ₂ system at 25 °C	82
Table B-33:	PRSV-HV-UNIQUAC predicted concentrations for Acetone/Acetaminophen/Phenanthrene/CO ₂ system at 25 °C	83
Table B-34:	UNIQUAC interaction parameter matrix for Acetone/Acetaminophen/Phenanthrene/CO ₂	83

LIST OF FIGURES

Figure 1.1:	Schematic comparison of properties of various solvent systems	2
Figure 1.2:	Qualitative flow chart for GXL processing	3
Figure 3.1:	Apparatus setup for expansion experiment	14
Figure 3.2:	Apparatus setup for fractional crystallization	18
Figure 3.3:	Volume expansion of experimental data taken in this Thesis	27
Figure 3.4:	Solubility calculated using Peng Robinson equations NMP is shown having the lowest mass based CO ₂ solubility. It will be shown later in this paper that the author's equations model the real system very well.	28
Figure 3.5:	Acetone VLE Experimental data from this work; Predicted equilibria calculated from the Peng-Robinson EOS model ($k=0.0114$); Experimental points from {Day, 1996/1999} and {Adrian, 1997}, both of which are used Analytical/sampling techniques.	29
Figure 3.6:	Figure 3.6: Acetonitrile VLE Experimental data from this work; Predicted equilibria calculated from the Peng-Robinson EOS model ($k=0.07$)	30
Figure 3.7:	N-Methyl Pyrrolidone VLE Experimental data from this work; Predicted equilibria calculated from the Peng-Robinson EOS model ($k=-0.013931$)	31
Figure 3.8:	Tetrahydrofuran VLE Experimental data from this work; Predicted equilibria from the Peng-Robinson EOS model ($k=0.0176$)	31
Figure 3.9:	Dichloromethane VLE Experimental data from this work; Predicted equilibria from the Peng-Robinson EOS model ($k=0.0553$)	32

Figure 3.10:	Nitromethane VLE Experimental data from this work; Predicted equilibria from the Peng-Robinson EOS model ($k = -0.049493$ and $l_{ij} = -0.0330751 = -l_{ji}$). In this case, it was necessary to use the second PR mixing rule, $b_{ij} = (b_i + b_j)/2 \times (1 - l_{ij})$, to accurately match the experimental data points.	32
Figure 3.11:	Plot of our work and the literature data from Dixon and Johnston 1991 for phenanthrene in toluene at 25 °C	33
Figure 3.12:	Mole fraction ratio of phenanthrene to toluene, measured in this work.	34
Figure 3.13:	The solubility of the phenanthrene in toluene, tetrahydrofuran, and acetone with CO ₂ . The calculated data is from the PRSV-HV-UNIQUAC model. All three experiments started at saturation. Tai and Cheng and measured the expansion/precipitation pressure point for the saturated toluene/phenanthrene system at 35 ± 5 bar {Tai, 1998}. All data points were taken from this work.	35
Figure 3.14:	The solubility of the phenanthrene vs. the solubility of carbon dioxide in toluene, tetrahydrofuran, and acetone. The calculated data is from the PRSV-HV-UNIQUAC model. All data points were taken from this work.	35
Figure 3.15:	The solubility of the acetaminophen in acetone and ethanol mixtures with CO ₂ . The calculated data is from the PRSV-HV-UNIQUAC model. Both experiments started at saturation. The saturation concentrations were obtained from the literature {Granberg, 1999}. The other points were from this work. Tai and Cheng and measured the expansion/precipitation pressure point for the saturated ethanol/acetaminophen system at 48 ± 4 bar {Tai, 1998}.	37
Figure 3.16:	The solubility of the acetaminophen versus the solubility of carbon dioxide in acetone and ethanol. The calculated data is from the	37

PRSV-HV-UNIQUAC model. All points from this work.

- Figure 3.17: A PRSV-HV-UNIQUAC calculation of the phenanthrene concentration in a Toluene/CO₂/Phenanthrene/Acetaminophen (Quaternary) and the Toluene/CO₂/Phenanthrene (Ternary) system. The quaternary solution mole fraction was calculated using the moles of toluene, CO₂, and phenanthrene only. 40
- Figure 3.18: Quaternary runs of toluene/phenanthrene/acetaminophen/CO₂ at 25 °C. The first quaternary system was done as within approximately 10% of the saturation concentration. The second quaternary system was not at saturation. These calculations were conducted using the only moles of the toluene, CO₂, and phenanthrene. The calculated results were obtained from the PRSV-HV-UNIQUAC model. 41
- Figure 3.19: The PRSV-HV-UNIQUAC calculated solubilities of the phenanthrene and acetaminophen in a toluene/CO₂ system. 42
- Figure 3.20: The PRSV-HV-UNIQUAC calculated solubilities of the acetaminophen/acetone in the quaternary and the ternary systems. The solubility of acetaminophen in the quaternary system was calculated using only the moles of acetone, CO₂ and the acetaminophen. 42
- Figure 3.21: The PRSV-HV-UNIQUAC calculated solubilities of the phenanthrene/acetone in the quaternary and the ternary systems. The solubility of acetaminophen in the quaternary system was calculated using only the moles of acetone, CO₂ and the phenanthrene. 43
- Figure 3.22: Quaternary runs of acetone/phenanthrene/acetaminophen/CO₂ at 25 °C. The quaternary system was run with a dilute solution. These calculations were conducted using the only moles of the toluene, CO₂, and phenanthrene. The calculated results were obtained from the PRSV-HV-UNIQUAC model. All points were taken 44

from this work.

Figure 3.23:	Quaternary runs of acetone/phenanthrene/acetaminophen/CO ₂ at 25 °C. The first quaternary system was run with a dilute solution. These calculations were conducted using the only moles of the toluene, CO ₂ , and phenanthrene. The calculated results were obtained from the PRSV-HV-UNIQUAC model.	44
Figure A-1:	Drawing of Jerguson Cell system for phase equilibria	49
Figure A-2:	Picture of Solid Solubility apparatus, Jerguson Cell, sampling valves, EtAc Pump, Heater/Fan	50
Figure A-3:	Close up of Jerguson cell	51
Figure A-4:	Encircled: Pole connected to the Jerguson cell This mounts the cell approximately 30 cm	53
Figure A-5:	The valve connections series	54
Figure A-6:	The two 6-port valves connection (all 0.15mm ID tubes) are shown and outlined in this picture with following color coding: Line to sample; sample loop; waste/vent line; line to sampling valve; line to EtAc pump.	55
Figure A-7:	The water bath with the line from the sampling 6-port valve colored.	55
Figure A-8:	A schematic of the 6-port sampling valve	61
Figure B-1:	Jerguson Cell Volume Calibration	64
Figure B-2:	Solubility of carbon dioxide vs. Pressure for the various solvents used in this thesis	69
Figure B-3:	Gas chromatograph calibration of acetaminophen in ethyl acetate	73
Figure B-4:	Gas chromatograph calibration of phenanthrene in ethyl acetate	74
Figure B-5:	Gas chromatograph calibration of ethanol in ethyl acetate	74

Figure B-6:	Gas chromatograph calibration of toluene in ethyl acetate	74
Figure B-7:	Gas chromatograph calibration of acetone in ethyl acetate	75
Figure B-8:	Gas chromatograph calibration of tetrahydrofuran in ethyl acetate.	75
Figure C-1:	Bubble Point Calculation Flow Sheet	84

LIST OF SYMBOLS

Abbreviations

CED: Cohesion Energy Density

DCM: Dichloromethane

EOS: Equation of State

EtAc: Ethyl Acetate

GXL: Gas-Expanded Liquid

MOSCED: Modified Separation of Cohesive Energy Density Model

NMP: N-methyl pyrrolidone

PRSV-HV-UNIQUAC: Peng-Robinson-Styrjek-Vera equation of state with UNIQUAC based Huron-Vidal

SCF: Supercritical Fluid

THF: Tetrahydrofuran

UNIQUAC: Universal Quasi-Chemical theory

Letters

A: Cross-sectional area of a pipe

a,b: Peng-Robinson constants

C: Peng Robinson Huron-Vidal constant

ΔC_p : heat capacity of a chemical

D: diffusion coefficient of a substance in a fluid

\underline{G} : Gibbs Free Energy of the system

G^E : Excess Gibbs Free Energy

\underline{G}^{IG} : Ideal gas conditions Gibbs free energy

F : Force put on a fluid

f_i^L, f_i^V : fugacity of component (i) in the liquid and vapor phase respectively

ΔH_{fus} : heat of fusion of a chemical

k : constant in calculation of a in Peng Robinson Huron-Vidal EOS

k_B : Boltzman constant

k_{ij}, l_{ij} : binary interaction parameters

P^0 : initial pressure of system

P : pressure of fluid

P_{ci} : critical pressure of component (i)

P^{sat} : saturation pressure of component (i)

q_i : surface area parameter of component (i)

R^0 : radius of solute particle

R : ideal gas constant

r_i : volume parameter of component (i)

T : temperature

T_{ci} : critical temperature of component (i)

T_m : melting point of a solute

T_{ri} : reduced temperature of component (i)

u_{ij} : average interaction energies of component (i) and (j) in UNIQUAC

v : velocity

V : total volume of the liquid

\underline{V} : molar volume of the fluid

\bar{v}_i^{-L} : partial molar volume of component (i)

x_i : mole fraction of component (i) in the liquid phase

x_{ideal} : ideal solubility of a solid solute

y : radial ordinate in a pipe

y_i : mole fraction of component (i) in the vapor phase

z_i : mole fraction of component (i) in either vapor or liquid phase

Greek Symbols

α : temperature component in constant a of Peng Robinson EOS

α_i : acidity of component (i)

β_i : basicity of component (i)

Δ : difference

Φ_i : volume fraction of component (i)

ϕ_i^L, ϕ_i^V : fugacity coefficient of component (i) in the liquid and vapor phase respectively

ϕ_i^{sat} : fugacity coefficient of component (i) at the saturation pressure

γ : activity coefficient of component (i)

λ_i : polarizability of component (i)

μ : viscosity

θ_i : area fraction of component (i)

τ_i : polarity of component (i)

τ_{yx} : shear stress on a fluid

ω : acentric factor of component (i)

ψ, ξ : *asymmetry terms*

SUMMARY

The work conducted in this thesis is two-fold. First, binary vapor liquid equilibria of several solvent/CO₂ systems are measured at 40 °C. The systems analyzed are all gas-expanded liquids (GXLs) characterized with a Jerguson Cell apparatus. A Jerguson cell is a windowed pressure vessel that allows one to measure the height of the condensed liquid. Using this height and the known overall contents in the cell, one can calculate the liquid composition without using any external sampling.

Secondly, this same setup is attached to a sampling system, and solid solubility (fractional crystallization) is measured for various GXL systems. The CO₂ acts as an antisolvent in what is commonly known as a gaseous antisolvent (GAS) system. Essentially, this work shows that expansion of the tested solvents with CO₂ will cause the precipitation of the solid solute. This work also analyzes the affect two solutes have on each other in a quaternary GAS system.

Gas-expanded liquids combine desirable gaseous properties and liquid properties to yield a very useful solvent for many applications. An advantage of GXLs is that a relatively small change in pressure or temperature can greatly affect the solvation properties. The tunability of GXLs increases as the amount of the gas (usually CO₂) increases in the liquid phase. With the benign chemical nature and environmental impact of CO₂ processing, GXLs and supercritical fluids (SCFs) have garnered a lot of attention for industry and academia. Supercritical fluids in this work refer to pure CO₂ above its critical temperature and pressure.

CHAPTER 1

INTRODUCTION

This work measures the phase equilibria (vapor-liquid composition) at a specified temperature and pressure and the expansion of organic liquids when solvated with carbon dioxide. This type of system is called a gas-expanded liquid (GXL). Equipment and projects involving GXLs cannot be designed without knowledge of GXL phase equilibria and volume expansion. An advantage of the method used in this work over many past phase equilibria experiments is that liquid and vapor compositions are deduced from the height of liquid level (Synthetic Method) rather than the use of outside sampling (Analytical Method).

This work also investigates the use of GXLs for fractional crystallization at room temperature. A chemical process may necessitate separating solid components from one another in a mixture. Of the many types of separations, the one that exploits the difference in melting points and heats of fusion of the solutes is fractional crystallization. Common industrial crystallization processes such as freezing typically involve a rigorous use of energy. Systems investigated in this work involve organic solvents with one and two solutes with the gas acting as the antisolvent. The solvent power of a liquid decreases as carbon dioxide expands the liquid in a process known as a Gas Antisolvent (GAS) system. Figure 1.1 shows that the solvent power decreases as well as an increase in the transport ability (lower viscosity) of GXLs compared to organic liquids.

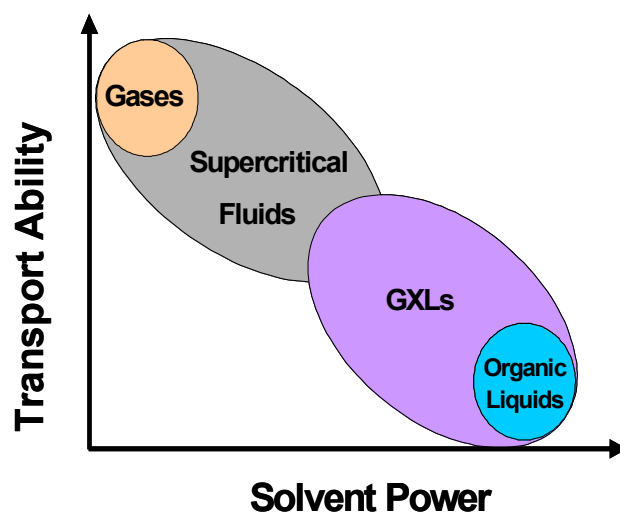


Figure 1.1: Schematic comparison of properties of various solvent systems

Where GXLs are essentially a liquid with a gas dissolved therein, supercritical fluids (SCFs) are typically a pure gas above its critical temperature and/or pressure. GXL and SCF processing typically use carbon dioxide as the gas or supercritical fluid. Carbon dioxide is useful because its critical temperature is near room temperature (30 °C), and it is non-toxic, inflammable, as well as naturally abundant.

The properties of GXLs and SCFs give them a clear advantage over traditional organic solvents. Unlike many basic liquid mixtures, which require a physical change of the composition to appreciably affect its properties, GXL and SCF properties can be changed by adjusting the pressure and/or temperature of the system. However, GXLs require lower operating pressures than SCFs in similar systems.

With the ability of GXLs and SCFs to tune the solvating power of a system, the separation process is easier to manipulate in order to achieve the desired process specifications. Most GXL and SCF processes usually involve pressurizing a system to

conduct a process and then depressurizing the system for extraction of the product. The qualitative flow chart in Figure 1.2 illustrates this process:

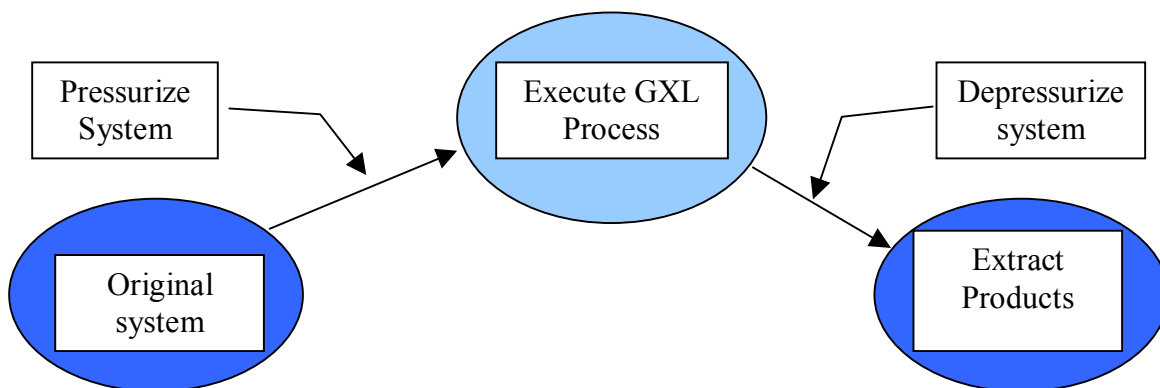


Figure 1.2: Qualitative flow chart for GXL processing

A possible disadvantage of GXL and SCF processing is the requirement of precise process control. However, there are significant gains: reusing CO₂ and solvent offers significant budgetary saving, manufacturing processes can be optimized, and laboratory (or plant) safety will be increased. Examples of different GXL and SCF processes are referenced in Chapter 2.

There has also been a push, originating around the late 1960s, for increasingly environmentally sensitive methods of manufacturing. GXLs have been shown to reduce the necessity of environmentally dangerous organic solvents and use naturally abundant carbon dioxide, thus GXL processing has also been labeled an environmentally sound process.

CHAPTER 2

LITERATURE REVIEW

The application of GXLs and SCFs for fractional crystallization has been studied rather extensively in the literature. As a result, there have been several different types of crystallization methods developed over the years, such as gaseous antisolvent (GAS) systems and Rapid-Expansion of Supercritical Solutions (RESS) {Kayrak, 2003} {Diefenbacher, 2002}. Other types of systems include Particle Generation from Gas Saturated Solutions (PGSS) {Kikic, 1997}, and the numerous methods outlined by Jung {Jung, 2001}. In all of these cases, carbon dioxide acts as an antisolvent for the solid. The solubility of the various heavy components in gas-expanded liquids have also been measured with success {Ventosa, 2003} {da Rocha, 1996}.

Supercritical fluid antisolvent processes have shown that one can obtain micro- and nano-scale particles from solid solutes with a narrow particle size distribution {Fusaro, 2004} {Hong, 2000} {Kayrak, 2003}. The small particles and uniform size distribution are absolutely necessary in the production of pharmaceuticals and other fine chemicals. Lastly, a few articles have considered the scale-up and economics of using these pressurized systems for industrial production {Subra, 2000} {Perrut, 2000} {Thiering, 2001}.

When dealing with expansion and phase equilibria, many authors have conducted experiments using various methods. The review article by Christov and Dohrn has an extensive list of articles about binary and multiphase systems with phase equilibria measurements {Christov, 2002}.

Other applications include the use of near-critical and supercritical CO₂ to extract vitamins and/or oils from natural sources {Mukhopadhyay M., 2003} {Odabasi, 2002} {Bravi, 2002} {Bozan, 2002}. Supercritical CO₂ has also been used for the extraction of caffeine from coffee beans {van der Stegen, 1977}.

For many years, supercritical CO₂ has been instrumental in the recovery of petroleum from oil deposits buried deep within the earth {Wellington, 1982} {Miura, 2003} {Kubatova, 2002}. The supercritical carbon dioxide is pumped into the base of the reservoir to raise the oil level. More recently, some petroleum research has been geared toward sequestering and modeling the geological path of the CO₂ that was pumped into these reservoirs {Pawar, 2003} {Westrich}. Also, researchers have explored injecting carbon dioxide into crude petroleum and petroleum derivatives for extraction and separation {Hwang, 1995} {Hawthorne, 1993} {Huang, 1990}.

SCF's and GXL's properties of high vapor pressure, low viscosity, and low density, have made equipment cleaning an attractive application as well {Laube, 2001} {Weber, 1995}. The ease with which GXLs can penetrate nano-scale ditches and corners has made GXLs a useful alternative to traditional cleaning solvents for silicon wafers in microelectronics processing {Spuller, 2004} {Myneni, 2002} {Weibel, 2002} {Levitin, 2004} {Dostal, 2002}. Work has been done in purification of Natural Gas liquid streams using crystallization of the heavier hydrocarbons {Jensen, 2003} {Abdulkadirova, 1997} {Marteau, 1996} {Miura, 2003}.

Several review articles have been written which further discuss the use of GXLs for reaction mediums, homogeneous catalysis, separations, and other applications {Marr, 2000} {Hauthal, 2001} {West, 2001} {Beckman, 2004}. Authors have also discussed

the scale-up and economic consideration of these experiments for specific industries {Smith, 1998} {Cygnarowicz-Provost, 1996} {Montero, 1996}. According to the literature, there seems to be a lingering resistance to using high pressure carbon dioxide for chemical processing. One reason for this resistance is likely the perceived high cost of compression/release of CO₂ and the extensive cost of purchasing new equipment to integrate the new process. Therefore, more work must be done to make GXL/SCF processes more economical.

One of the primary concerns of chemical processing in all areas, from the laboratory, to the pilot plant, to the large-scale plant is safety for the worker. Using CO₂ in GXLs and SCFs delivers several advantages over the typical organic solvent. Carbon dioxide has a high vapor pressure (62 bar at room temperature), which means it will quickly vaporize if it ever leaks. With its inflammability and non-toxic characteristics, CO₂ does not pose a threat to anyone working with it, save the potential for explosions and/or asphyxiation that come with any high pressure system {Beckman, 2004}.

Many authors have tried to develop correlations to model phase behavior. These models are usually devised with the intention of predicting phase behavior of systems without physical experimentation. Several authors have made attempts to model phase equilibria using the chemical makeup of the mixture components, known as group-contribution calculations {Artal, 2001} {Blas, 2002} {Zhi-Yu, 2000}. Other authors have used various mixing rules and equation of state (EOS) calculations to compare experimental data to the predicted data. Knudsen, Stenby and Fredenslund and others have completed a comprehensive study on comparing the accuracy of various mixing rules to a few complex systems {Knudsen, 1993} {Orbey, 1996}. The literature also

shows that vapor liquid equilibria (VLE) data has been used to calculate mass transfer properties {Lin, 2003}.

CHAPTER 3

VAPOR-LIQUID BINARY PHASE EQUILIBRIA AND TERNARY/QUATERNARY SOLID SOLUBILITY SYSTEMS

Introduction

This research concerns phase equilibria and gaseous antisolvent systems. Phase equilibria models were found for various common organic solvents injected with carbon dioxide at various pressures. When pressurized carbon dioxide is dissolved in a solvent, a notable expansion is observed. This new solvent is called a gas-expanded liquid (GXL).

Binary Phase Equilibria

GXLs have several property advantages over customary organic solvents. One major property advantage is that the viscosity of an organic solvent typically decreases as it expands with injection of CO₂. This decrease in viscosity becomes more drastic as the pressure increases. Viscosity has a direct affect on fluid flow and mass transfer properties, illustrated in the fluid flow (Equation 3.1) and diffusion equations (Equation 3.2) respectively.

Newton's Law of viscosity is the equation for Newtonian fluid flow {Geankoplis, 1993}:

$$\tau_{yx} = \mu \frac{\partial v_x}{\partial y},$$

Equation 3.1

where the change in fluid velocity (v) over the change in radius or height (y) with viscosity (μ) representing the constant of proportionality, or the resistance to flow, and τ_{yx} represents the shear stress on the fluid.

The Stokes-Einstein equation is a standard for various correlations of diffusion coefficients {Hines, 1985}:

$$D = \frac{k_B T}{6\pi\mu R_0}.$$

Equation 3.2

Assuming the temperature remains constant, the viscosity of the solvent (μ) is the major factor in the change of diffusion coefficient (D). The Boltzman constant (k_B) and the radius of the solute particle (R_0) remain constant if the same solute is used.

GXLs have been examined for phase transfer catalysis, reaction mediums, or more generally speaking, as a tunable solvent. The solubility and viscosity of GXLs are heavily dependent on the pressure of the system. This is especially true as one approaches the critical pressure of CO₂ {Eckert, 2000}. In order to use a GXL for processing or experimentation, it is necessary to know the degree to which pressure affects the expansion and composition of the GXL; therefore, this research studies the GXL vapor-liquid equilibrium and expansion effect of CO₂ for various organic solvents. Many authors have done work on phase equilibria in the past and this thesis will discuss other methods of experimentation in comparison to the methods used here.

Fractional Crystallization

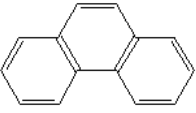
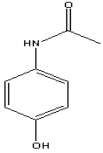
When designing a chemical process, two basic functions must be executed: reaction and separation. The reactions are typically developed in a laboratory setting and

are scaled up for industrial processes. The engineer scales up the reactor and then must develop a method to separate the product from the byproducts and/or solvents, which can number from one to several hundred. The separation involves discernment of the physical or chemical properties that make the product different from the unwanted byproducts or solvents. These differences can be used for separation process design, and there are certain processes that are more appropriate for exploitation of various property differences. For vast differences in solubility in a particular liquid, one can use a liquid-liquid extraction. For differences in boiling points, one can use a distillation process. For differences in melting points, fractional crystallization may be best.

This paper will demonstrate the solubility of a solid solute in several common solvents as well as the separation effects when a second solute is added to the system. Carbon dioxide acts as an antisolvent in the system. An antisolvent is material that is miscible with one component of a solution but immiscible with the other component(s) in the system. The method is generally called the gas antisolvent (GAS) system. Dixon and Johnston in 1991 did a similar study with both phenanthrene and naphthalene in toluene. Their work concluded that the two solids act as co-solvents for each other, thus slightly decreasing the amount of either component precipitated at the same pressure compared to solutions where only one solute is present.

The solutes used in this research are phenanthrene and acetaminophen (Tylenol). These solutes have melting points with a difference of 70 °C; thus, fractional crystallization is an ideal mode of separation.

Table 3.1: Thermal properties of phenanthrene and acetaminophen

Property	Phenanthrene	Acetaminophen
		
ΔH_{fus} (J/mol)	16500	27700
Melting Pt (°C)	99.4	168
ΔC_p (J/mol*K)	12	99.8
Ideal Solubility (mol frac)	0.276	0.0766

The ideal solubility of a particular solid is the same regardless of solvent and is calculated using the expression below {Sandler, 1999}:

$$x_{ideal} = \exp \left[\frac{-\Delta H_{fus}}{RT_m} \left(\frac{T_m}{T} - 1 \right) - \frac{\Delta C_p}{R} \left(\ln \frac{T_m}{T} - \frac{T_m}{T} + 1 \right) \right].$$

Equation 3.3

Phenanthrene is a solute that has been studied extensively in the literature for GXL and supercritical processing. Acetaminophen is a pharmaceutical that is used as an anti-pyretic. Acetaminophen is commonly used as a representative chemical when conducting pharmaceutical research. In pharmaceutical manufacturing, very small crystals and uniform size distribution are important product specifications. Due in part to the uniform and rapid mixing of CO₂ in GAS systems, GXLs/SCFs have proven to yield micro- and nano-scale crystal sizes with uniform size distribution {Shekunov, 2001} {Muhrrer, 2002} {Hong, 2000} {Warwick, 2000} {Kayrak, 2003} {Ventosa, 2003}.

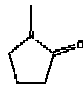
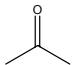
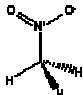
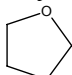
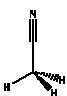
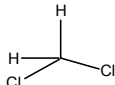
Experimental Design

Binary VLE Measurements

These solvents were chosen to measure the VLE for a number of reasons.

Acetone/CO₂ phase equilibria has been studied extensively in the literature, and thus the apparatus and methods in this thesis can be checked for validity. The other solvents are common organic solvents and are regularly used in research and industry, some of which have not been studied previously.

Table 3.2: Materials for the VLE experiments

Chemical	Supplier	Product Number	CAS Number	Purity
N-methyl-pyrrolidone 	Aldrich	270458	872-50-4	99%
Acetone 	Sigma-Aldrich	270725-2L	67-64-1	99.9+%
Nitromethane 	Aldrich	27042-3	75-52-5	98.7%
Tetrahydrofuran 	Sigma-Aldrich	186562-1L	109-99-9	99.9%
Acetonitrile 	Sigma-Aldrich	271004	75-05-8	99.8%
Dichloromethane 	Fisher	UN1593	75-09-2	Certified ACS
CO ₂	Airgas	UN1013	124-38-9	SFE/SFC Gr. 6.0

Equipment

The experiment was set up using a Jerguson cell as the pressurized vessel. The cell has a window and a ruler along its height allowing the researcher to see the contents in the cell and measure the expansion. The cell has a pole attached to its back to allow rotation of the entire cell for mixing. The cell has a stainless steel tube (0.4064-mm ID) connecting to a CO₂-containing syringe pump called an ISCO (Model 500D). Valves are attached to lines between the ISCO pump and the cell to control input with a pressure gauge placed on the tube between the cell and the ISCO pump. The ISCO pump is operated with a set pressure and is connected to a chiller to control the temperature of the CO₂, allowing the researcher to know the volume of CO₂ pumped into the cell. The cell itself is encased in a 92.3925 X 91.44 X 54.61 cm³ polycarbonate case with 0.9525-cm thick sheets, which functions as an air bath. A heater and a fan are also inside the casing, with the heater wired to a homemade Temperature Controller that acts as a thermostat to heat the airbath and maintain a temperature set point. The fan facilitates an even distribution of temperature in the airbath. Thermocouples are inside the cell and inside the case to control the temperature of the contents in the cell and the airbath. A vacuum pump (Fisher Scientific Maxima C Plus 701585) is attached using a valve to the same line connecting ISCO and the cell to allow evacuation of the pump for cleaning. Figure 3.1 illustrates the system described above.

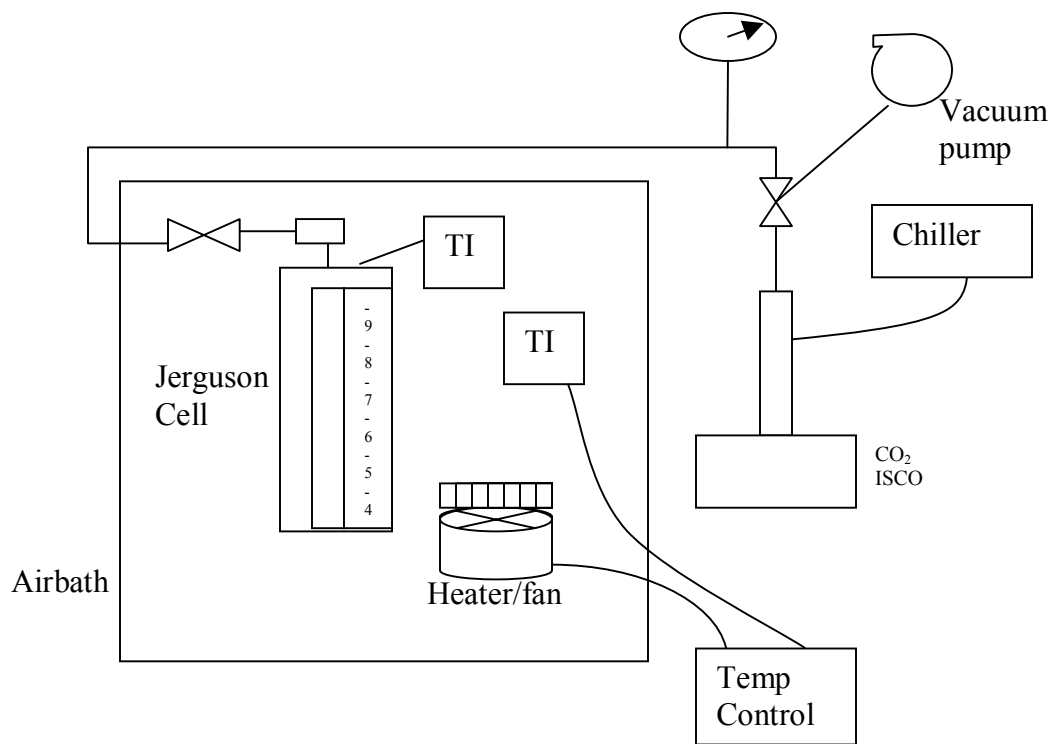


Figure 3.1: Apparatus setup for expansion experiment

The detailed assembly of the apparatus is explained in the Appendix A. The researcher used a mounted cathetometer (Gaertner Scientific Corporation: 3921-P) to observe the level of the liquid.

Calibrations

The volume of the cell was calibrated using water poured into the cell in known volume increments and the height was measured. To measure the volume of the entire system, the cell is evacuated with a vacuum pump and then pressurized with known moles of CO₂ from the ISCO. After the pressure in the cell stabilizes, the researcher can record the temperature (stabilized from temperature control) and pressure, and then get the molar density from the literature or a reliable equation of state. The cell volume

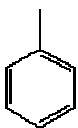
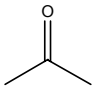

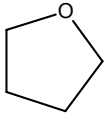
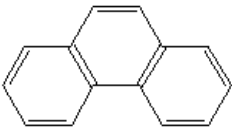
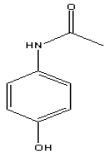
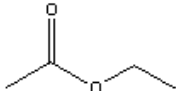
obtained from the CO₂ pressurization and the water level measurement will give the researcher the volumes of the liquid and vapor phases during normal experimentation. The cell calibration data is in Appendix B.

Phase Equilibria Measurement

The cell is first cleaned out with acetone and evacuated with the vacuum. The syringe full of the selected solvent (no air bubbles!) is then screwed into the cell valve and the desired amount of liquid (approximately 30-40 mL) is injected. The line to the ISCO is reconnected and re-evacuated before opening the cell valve. The valve is opened and the set temperature is set with the heater. After mixing, temperature and pressure will stabilize and the researcher can record the pressure, liquid level, and temperature. A detailed procedure is in Appendix A.

Fractional Crystallization

Table 3.3: Materials for fractional crystallization experimentation

Chemical	Supplier	Product Number	CAS Number	Purity
Toluene 	Sigma-Aldrich	244511-2L	108-88-3	99.8%
Acetone 	Sigma-Aldrich	270725-2L	67-64-1	99.9+%
Ethanol 	Aldrich	27764-9	64-17-5	
Tetrahydrofuran 	Sigma-Aldrich	186562-1L	109-99-9	99.9%
Phenanthrene 	Aldrich	P11409-500GA	85-01-8	98%
Acetaminophen 	Aldrich	A7302-250G-A	103-90-2	98%
Ethyl Acetate 	Fisher	UN1173	141-78-6	ACS Certified

Equipment

The Jerguson cell setup for the fractional crystallization is the same as the phase equilibria experiment save for the switching 6-port valve attached to the base of the cell. The cell itself is connected to the 6-port valve with a frit attached to the bottom of the cell. The frit keeps the solids from entering the 6-port valve. The valve contains a sample loop designed to allow a small amount of liquid from the cell, approximately 3 μL , to be analyzed. The 6-port valve has a connection to a pump (Eldex Laboratories, Inc, Model: AA-100-S) connected to a flask of ethyl acetate in order to rinse/flush the sample loop. The 6-port valve has a connection to another 6-port valve. This second valve has a connection to tube that leads to an inverted 25 mL buret in a water bath. For high pressures for which a large amount of CO_2 is in the GXL, an inverted 50 mL graduated cylinder was used. A second connection of the second 6-port valve goes to a 10 mL flask. The former connection is to sample the volume of the vapor phase, and the latter is to sample the liquid phase. Figure 3.2 provides a diagram of the system and a detailed breakdown of the apparatus is explained in Appendix A.

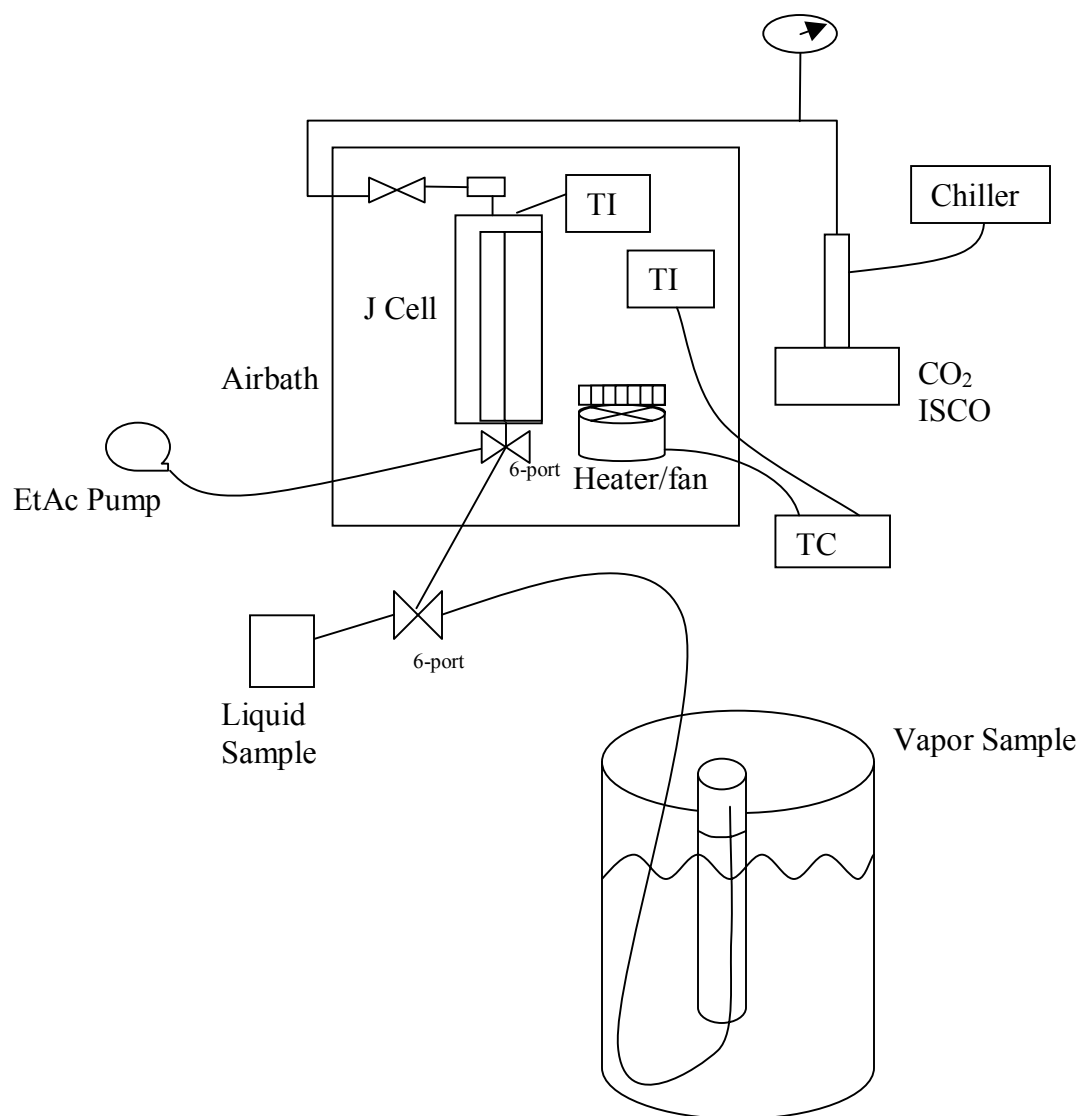


Figure 3.2: Apparatus setup for fractional crystallization

Fractional Crystallization Measurements

The initial solution (approximately 40 mL) is loaded into the cell in the same fashion as the phase equilibria experiment. The researcher heats the contents to a desired temperature and agitates the cell to facilitate mixing. The lines of the first and second 6-port valves are flushed with ethyl acetate before the sampling begins. The sample loop is charged with contents from the cell and then pumped to the liquid sampling or vapor sampling apparatus. For the liquid sample, the contents are put in a 1 mL gas chromatograph vial and analyzed in the gas chromatograph. The concentration of the organic solvent and the solute(s) in the liquid phase is measured in this analysis. The gas chromatograph was calibrated with experimental solutes and solvents in pure ethyl acetate. The vapor sampling was measured by the change in the level of water after sampling and flushing of the line. A detailed procedure of the sampling technique is presented in Appendix A.

Theory

Binary VLE Measurements

The phase equilibria measurements consisted of height liquid level, initial liquid volume, temperature, pressure, and volume of added CO₂. The volume of the liquid phase was found using the cell volume calibration curve. The volume expansion was calculated from the following expression {Kordikowski, 1995}:

$$\Delta V(\%) = \frac{V(P, T) - V(P^0, T)}{V(P^0, T)} \times 100\%,$$

Equation 3.4

where $\Delta V(\%)$ is the percentage of volume expansion, $V(P^0, T)$ is the liquid volume at zero pressure, and $V(P, T)$ is the liquid volume at the current pressure. The Peng-Robinson equation of state with quadratic mixing rules was used to find the vapor mole fraction (bubble point curve) using the liquid mole fraction {Peng, 1976}:

$$P = \frac{RT}{\underline{V} - b_m} - \frac{a_m}{\underline{V}(\underline{V} + b_m) + b_m(\underline{V} - b_m)},$$

$$a_m = \sum_{i=1}^n \sum_{j=1}^n z_i z_j a_{ij},$$

$$a_{ij} = \sqrt{a_{ii} a_{jj}} (1 - k_{ij}),$$

and

$$b_m = \sum_{i=1}^n z_i b_i (1 - l_{ij}),$$

Equation 3.5-3.8

where R (bar · cm³/mol · K) is the ideal gas constant; \underline{V} (cm³/mol) is the molar volume; P (bar) is the pressure of the system; T (K) is the temperature of the system; a , b are coefficients; k is the binary interaction parameter; z is the mole fraction in the liquid or vapor phase; subscripts i and j denote different components in the mixture; the equations for deriving parameters a and b for the mixture is from the quadratic or van der Waals mixing rules. The critical properties and acentric factor yield the coefficients a and b for the pure components.

The molar volume of the vapor phase was also calculated using the Peng-Robinson equation of state. Using the molar volume of the vapor phase, bubble point curve, and the volumes of CO₂ and liquid, the composition of the liquid and vapor phase is found for every pressure. The interaction parameters were adjusted to fit the data. A flow chart for the calculation steps is illustrated in Appendix C.

Equilibrium is reached when the fugacities (f) of each component in a system is equal in all phases. In this work, the predicted data was calculated using the *phi-phi* or equation of state method {Sandler, 1999}. In this method, both the CO₂ and the organic liquid are treated as if they were gases, therefore only the fugacity coefficients were found for both fluids in both phases:

$$f_i^L(T, P, \underline{x}) = f_i^V(T, P, \underline{y}),$$

and

$$x_i \phi_i^L P = y_i \phi_i^V P,$$

Equation 3.9-3.10

where x_i is the liquid phase mole fraction of component i ; y_i is the vapor phase mole fraction of component i ; ϕ_i is the fugacity coefficient of component i ; and superscripts L

and V denote liquid phase and vapor phase respectively. The liquid mole fraction is then varied to obtain the correct pressure and satisfy the fugacity expression.

The predicted data used the Peng-Robinson equation, utilizing the same mixing rules and interaction parameters {Sandler, 1999}.

Fractional Crystallization Prediction

A sampling of the liquid phase in the gas chromatograph and the vapor sampling using an inverted buret allows for direct calculation of the liquid phase composition, so no equations of state were used in finding the experimental data points. Thus, this is an Analytical method of experimentation. The liquid composition is of interest because the vapor phase is at least 98% carbon dioxide for pressures above five bars.

The solid solubility experiments are more complex to model than the binary fluid system. The gamma-phi method {Sandler, 1999} was used to determine the phase equilibria. It is assumed that solids are not present in the vapor phase due to the low vapor pressures of phenanthrene and acetaminophen. It is also assumed that the solid phase is pure. This method calculates the liquid side of the fugacity expression using activity coefficients and saturation fugacity coefficients and pressures. A summation of all the liquid fugacities was solved to calculate the specified pressure:

$$f_i^L(T, P, \underline{x}) = f_i^V(T, P, \underline{y}),$$

$$x_i \gamma_i \phi_i^{sat} P_i^{sat} \exp \left(\int_{P^{sat}}^P \frac{v_i^L}{RT} \right) = y_i \phi_i^V P,$$

and

$$\sum x_i \gamma_i \phi_i^{sat} / \phi_i^V P_i^{sat} \exp \left(\int_{P^{sat}}^P \frac{-\bar{v}_i}{RT} dP \right) = P,$$

Equation 3.11-3.13

The fugacity coefficients were calculated using the Peng-Robinson-Stryjek-Vera equation of state with the UNIQUAC-based Huron-Vidal mixing rule. The Huron-Vidal mixing rule is a composition based mixing rule {Stryjek, 1986} {Huron, 1979}:

$$a_m = b_m \left[\sum_i x_i \frac{a_i}{b_i} + \frac{G^E}{C} \right],$$

Equation 3.14

where $a_{m,i}$ and $b_{m,i}$ are the parameters to the Peng-Robinson EOS. With the Stryjek and Vera modification, $C = -0.62$. This factor is deduced from the requirement that the excess Gibbs free energy (G^E) of the solution found from the equation of state at infinite pressure should equal the actual infinite pressure excess Gibbs Free Energy $G^{E\infty}$ {Stryjek, 1986b}. The parameters for the individual components are calculated using the pure components' pure critical properties using the following series of equations {Ioannidis, 2001}:

$$a_i = 0.457235 \times \frac{R^2 T_{ci}^2}{P_{ci}} \alpha_i(T)$$

and

$$b_i = 0.077796 \times \frac{RT_{ci}}{P_{ci}}$$

Equations 3.15-3.16

where

$$\alpha_i(T) = \left[1 + \kappa_i(1 - T_{ri}^{0.5})\right]^2,$$

$$\kappa_i = \kappa_{oi} + \kappa_{li}(1 - T_{ri}^{0.5})(1 + T_{ri}^{0.5})(0.7 - T_{ri}),$$

and

$$\kappa_{oi} = 0.378893 + 1.4897153\omega_i - 0.1713184\omega_i^2 + 0.0196544\omega_i^3,$$

Equations 3.17-3.19

where T_r is the reduced temperature (T/T_c); and κ_{li} is a component dependent constant. In this work, the κ_{li} was fit to the known vapor pressure of the pure component. The excess Gibbs Free Energy (G^E) was correlated from the UNIQUAC {Abrams, 1975} correlation

below. The Poynting factor $\left(\exp\left(\int_{P^{sat}}^P \frac{\bar{v}_i}{RT}\right)\right)$ was calculated for each component, with the

partial molar volume (\bar{v}^L) assumed equivalent to the molar volume (\underline{v}^L). This

assumption corresponds to the fact that the Poynting factor typically stays close to unity.

This model will be denoted as: PSRV-HV-UNIQUAC for the remainder of the paper.

The activity coefficients were also found using the UNIQUAC modeling system

{Sandler, 1999} {Abrams, 1975}:

$$\begin{aligned}
\left(\frac{G^E}{RT}\right) &= \ln \gamma_i = \ln \gamma_i(\text{combinatorial}) + \ln \gamma_i(\text{residual}), \\
\ln \gamma_i(\text{combinatorial}) &= \ln \frac{\Phi_i}{x_i} + \frac{z}{2} q_i \ln \frac{\theta_i}{\Phi_i} + l_i - \frac{\Phi_i}{x_i} \sum_j x_j l_j, \\
\ln \gamma_i(\text{residual}) &= q_i \left[1 - \ln \left(\sum_j \theta_j \tau_{ji} \right) - \sum_j \frac{\theta_j \tau_{ij}}{\sum_k \theta_k \tau_{kj}} \right], \\
\theta_i &= \frac{x_i q_i}{\sum_j x_j q_j}, \\
\Phi_i &= \frac{x_i r_i}{\sum_j x_j r_j}, \\
l_i &= (r_i - q_i)z/2 - (r_i - 1), \\
&\text{and} \\
\ln \tau_{ij} &= \frac{(u_{ij} - u_{jj})}{RT}
\end{aligned}$$

Equations 3.20-3.26

where r_i is the volume parameter for component i , q_i is the surface area parameter for component i , θ_i is the area fraction of species i , and Φ_i is the volume fraction of species i . The average interaction energies (u_{ij}) were found by fitting the activity coefficients at infinite dilution ($\ln \gamma_i^\infty$ when $x_i \rightarrow 0$) from UNIQUAC to that from the Modified Cohesive Energy Density (MOSCED) model. The MOSCED is an equation system that takes into account the polarizability (λ term), dipolarity (τ term), hydrogen bonding (α, β term), size difference (v term) and asymmetry (ψ, ξ variables) of two components in solution to ascertain the infinite dilution activity coefficient each component in the other {Thomas, 1984}:

$$\ln \gamma_2^\infty = \frac{v_2}{RT} \left[(\lambda_1 - \lambda_2)^2 + \frac{q_1^2 q_2^2 (\tau_1 - \tau_2)^2}{\psi_1} + \frac{(\alpha_1 - \alpha_2)(\beta_1 - \beta_2)}{\xi_1} \right] + \ln \left(\frac{v_2}{v_1} \right)^\infty + 1 - \left(\frac{v_2}{v_1} \right)^\infty$$

and

$$\tau_T = \tau_{293} \left[\frac{293}{T} \right]^{0.4}; \alpha, \beta = \alpha_{293}, \beta_{293} \left[\frac{293}{T} \right]^{0.3}$$

Equations 3.27-3.29

Lastly, the solid solubility in the liquid must be determined. Using the heat of fusion and the melting point of the solid, the ideal solid solubility is found {Sandler, 1999}. The real solubility is found using the activity coefficient (from UNIQUAC) of the solid in the solution:

$$x_{si} = \frac{1}{\gamma_{si}} \exp \left[\frac{-\Delta H_{fus}}{RT_m} \left(\frac{T_m}{T} - 1 \right) - \frac{\Delta C_p}{R} \left(\ln \frac{T_m}{T} - \frac{T_m}{T} + 1 \right) \right]$$

Equation 3.30

The advantage that this method of calculation has over others is its lack of interaction parameters (“fudge factors”). These parameters are typically adjusted to fit data and can be difficult to obtain for complex systems, such as the ones analyzed in this thesis.

Results and Discussion

Binary Phase Equilibria: Comparison to Literature and Predicted Results

The volume expansion of the liquid phase for the different solvents is shown in Figure 3.3.

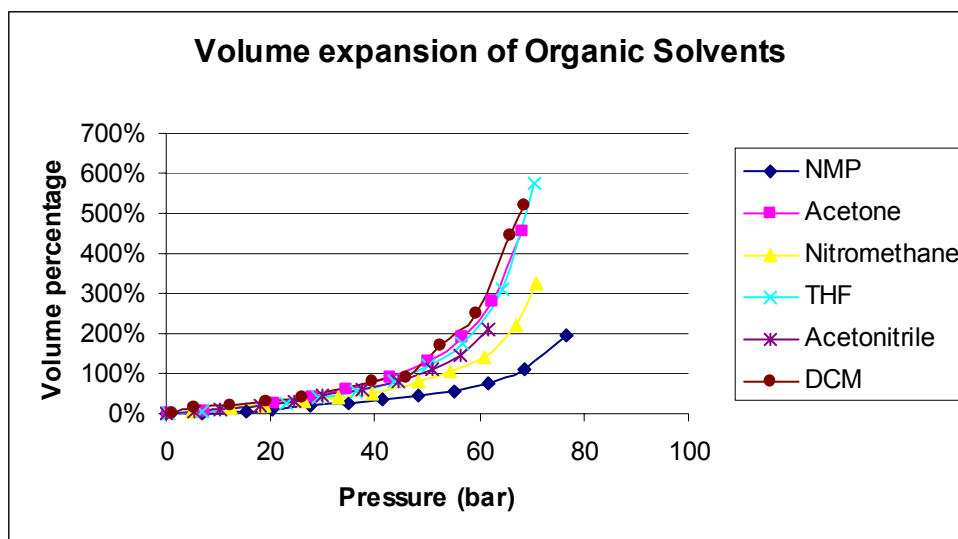


Figure 3.3: Volume expansion of experimental data taken in this thesis

Some solvents apparently expand more than others. At 70 bar, the expansion of n-methyl pyrrolidone (NMP) is 100% its original volume, while Tetrahydrofuran (THF), acetone, dichloromethane (DCM), and acetonitrile range from 580% to 450%. In a qualitative sense, the degree to which a solvent expands at a specified temperature and pressure tend to be dependent on its solubility with CO₂ (Figure3.4).

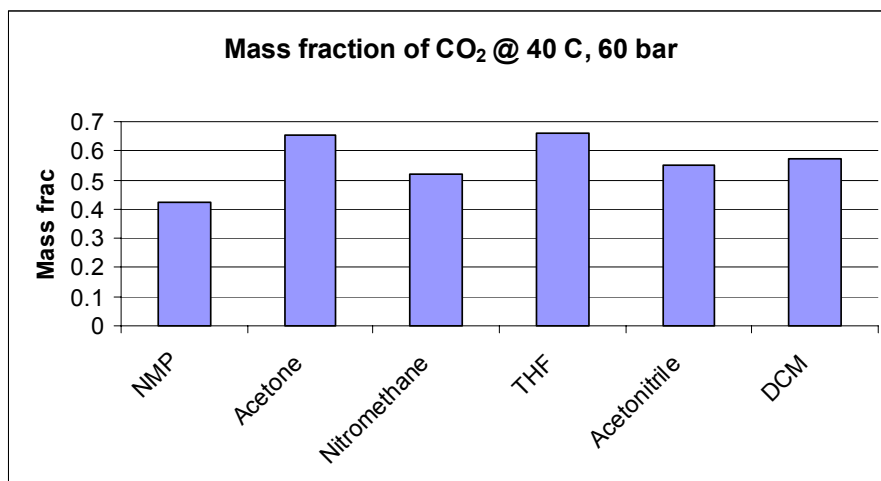


Figure 3.4: Solubility calculated using Peng Robinson equations. NMP is shown having the lowest mass based CO₂ solubility. It will be shown later in this paper that the author's equations model the real system very well.

Solubility is qualitatively related to components' chemical properties. For non-polar molecules cohesive energy density describes their solubility behavior accurately. Cohesive energy density is defined as “the energy of vaporization in calories per cubic centimeter, and is a direct reflection of the degree of van der Waals forces holding the molecules of the liquid together” {Burke, 1984}. Other forces like hydrogen bonding and polarity can come into play for the solubility of CO₂ in a liquid. Authors that analyze chemical group contributions and modifications and solvent cohesive energy density to predict solubility and expansion further analyze this phenomenon as it relates to GXLs {Blas, 2002} {Zhi-Yu, 2000} {Elvassore, 2002} {Thomas, 1984} {Artal, 2001}. The binary phase equilibria experiments were conducted, demonstrating excellent agreement with the predicted results (Figure 3.5).

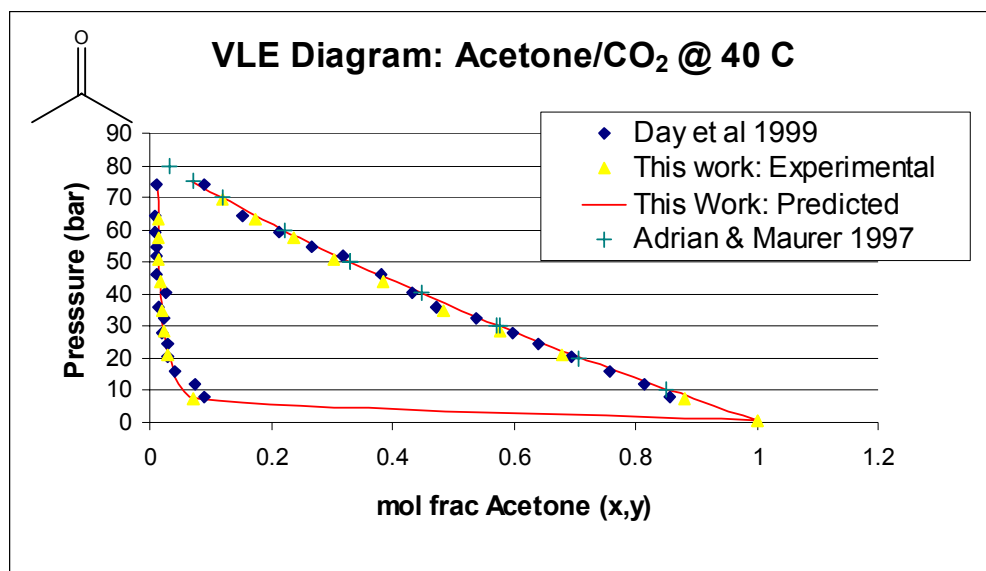


Figure 3.5: Acetone VLE Experimental data from this work; Predicted equilibria calculated from the Peng-Robinson EOS model ($k=0.0114$); Experimental points from {Day, 1996/1999} and {Adrian, 1997}, both of which are used Analytical/sampling techniques..

Figures 3.5 and 3.6 show excellent agreement with the past work of other researchers and the predicted EOS calculations with the data collected in this work. Neither Day et. al. nor Adrian and Maurer provide a reason in the literature why their equilibria data curves have slight scatter, as is evident in Figure 3.5. Since both sources utilize an external sampling of their GXLs in a gas chromatograph, there is a chance for minor error during the physical sampling of the system contents. However, the data agreement provides confidence that the apparatus and measurement techniques detailed in this paper work well.

Figures 3.6 through 3.10 show that GXLs analyzed in this work are in agreement with the phi-phi model for equilibrium as well as that of past experiments. For all of these data the temperature was $40\text{ }^{\circ}\text{C} \pm 0.2\text{ }^{\circ}\text{C}$. The pressure gauge was calibrated to approximately 0.1 psia or 0.034 bar. The volume calibration yielded a straight series of

curves. The error on all the measurements is no larger than 2%. For all the VLE data, all the second binary interaction parameters (l_{ij}) were insignificant. Nitromethane was the only exception. Nitromethane is considerably more polar than the other molecules, thus it is more difficult to match with this version of the Peng-Robinson EOS.

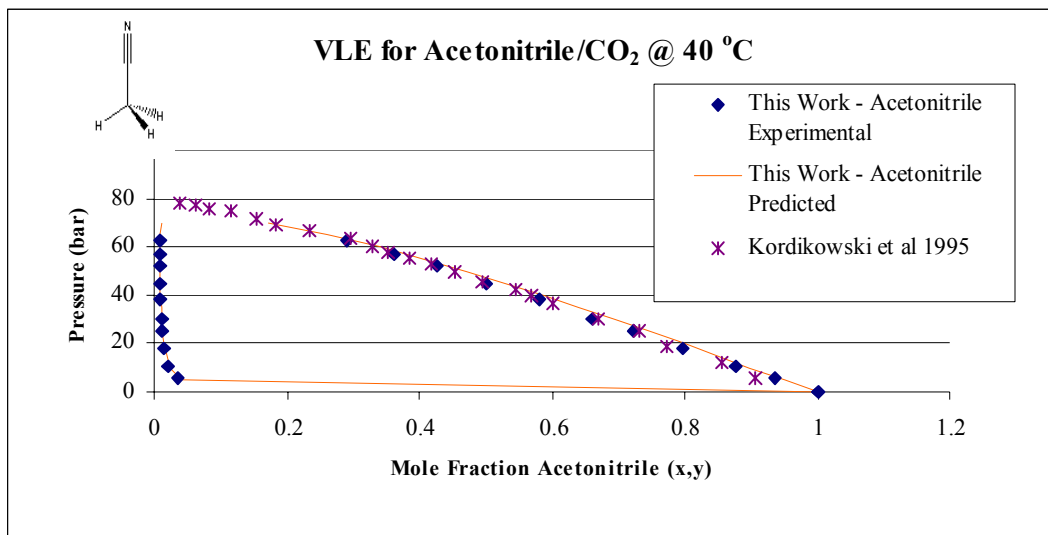


Figure 3.6: Acetonitrile VLE Experimental data from this work; Predicted equilibria calculated from the Peng-Robinson EOS model ($k=0.07$)

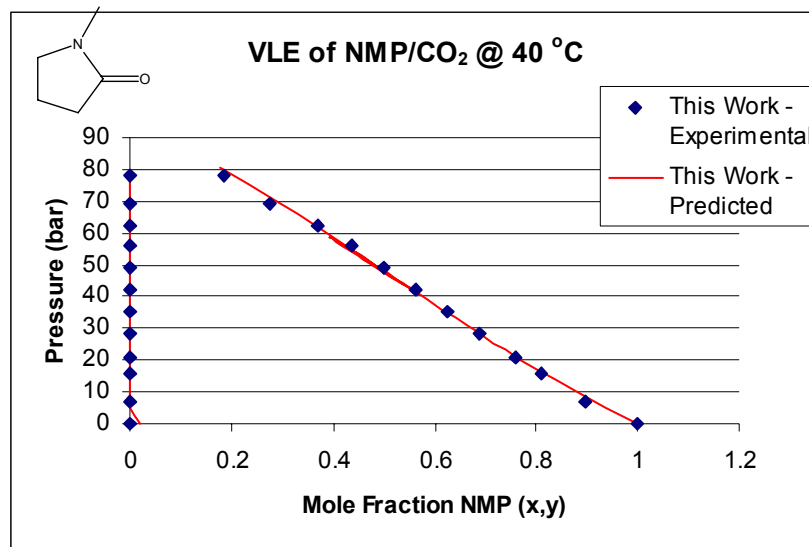


Figure 3.7: N-Methyl Pyrrolidone VLE Experimental data from this work; Predicted equilibria calculated from the Peng-Robinson EOS model ($k=-0.013931$)

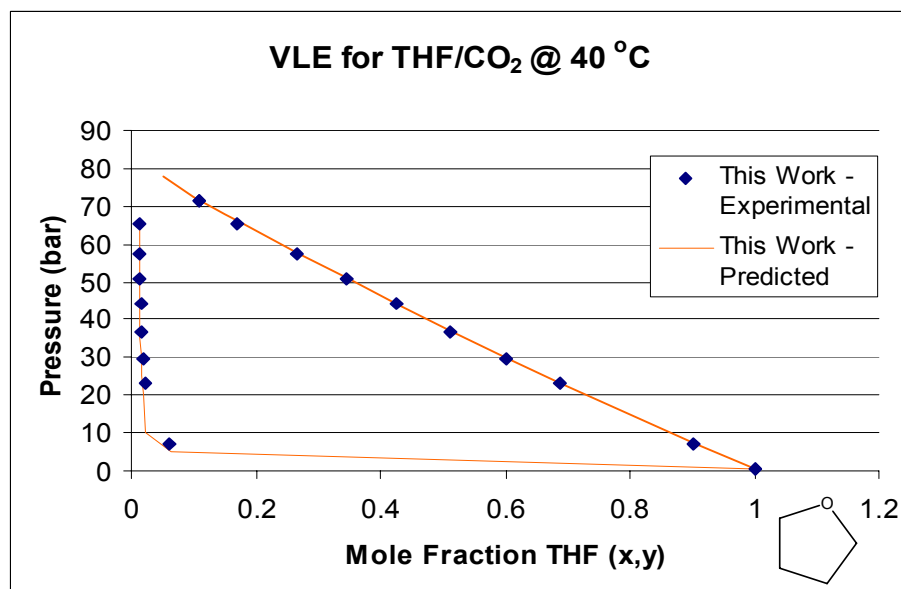


Figure 3.8: Tetrahydrofuran VLE Experimental data from this work; Predicted equilibria from the Peng-Robinson EOS model ($k=0.0176$)

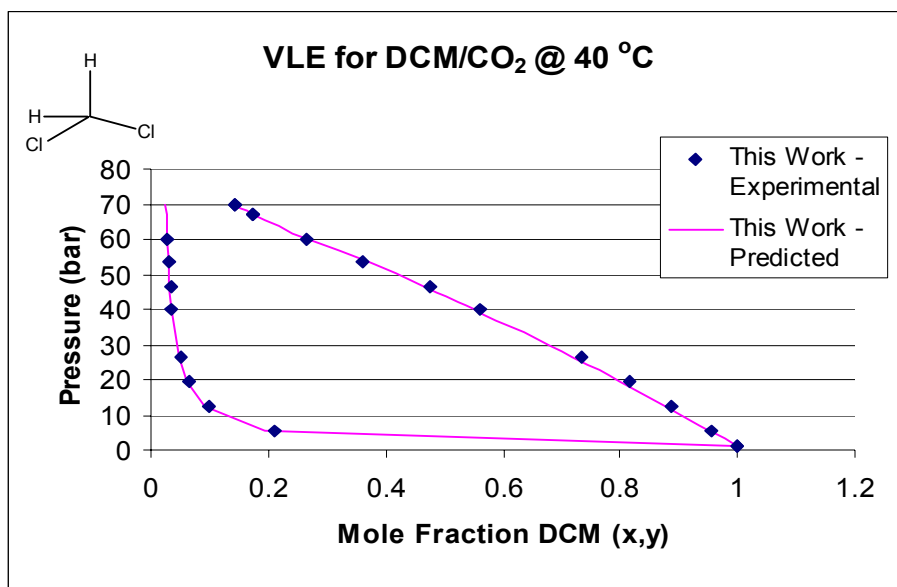


Figure 3.9: Dichloromethane VLE Experimental data from this work; Predicted equilibria from the Peng-Robinson EOS model ($k=0.0553$)

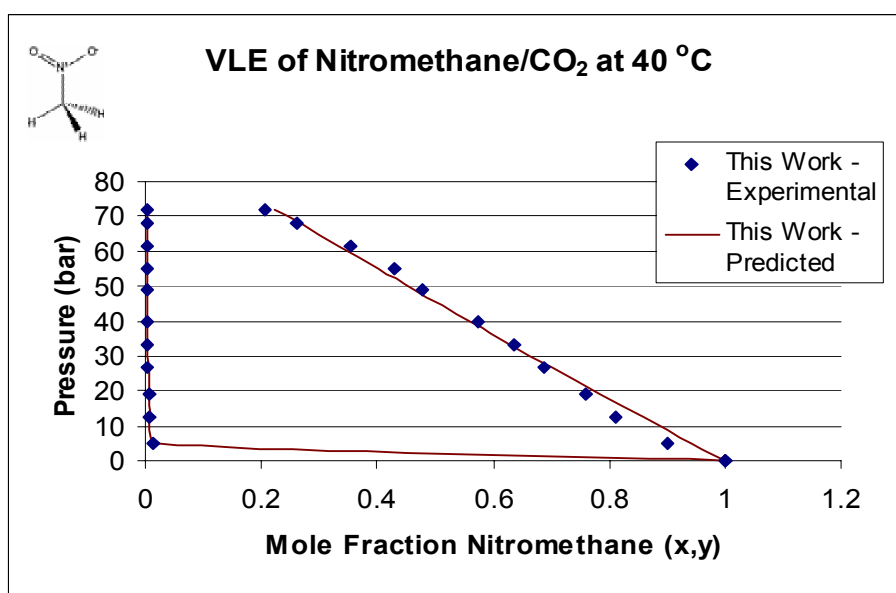


Figure 3.10: Nitromethane VLE Experimental data from this work; Predicted equilibria from the Peng-Robinson EOS model ($k = -0.049493$ and $l_{ij} = -0.0330751 = -l_{ji}$). In this case, it was necessary to use the second PR mixing rule, $b_{ij} = (b_i + b_j)/2 \times (1 - l_{ij})$, to accurately match the experimental data points.

Fractional Crystallization: Comparison to Literature and Predicted Data

As was stated in Chapter 2, several methods of crystallization using CO₂ as an antisolvent have been investigated throughout academia. To validate the process described in this paper for solid solubility measurements, experimental runs were conducted with the toluene and phenanthrene, the same components as Dixon and Johnston, 1991. The results are illustrated in Figure 3.11.

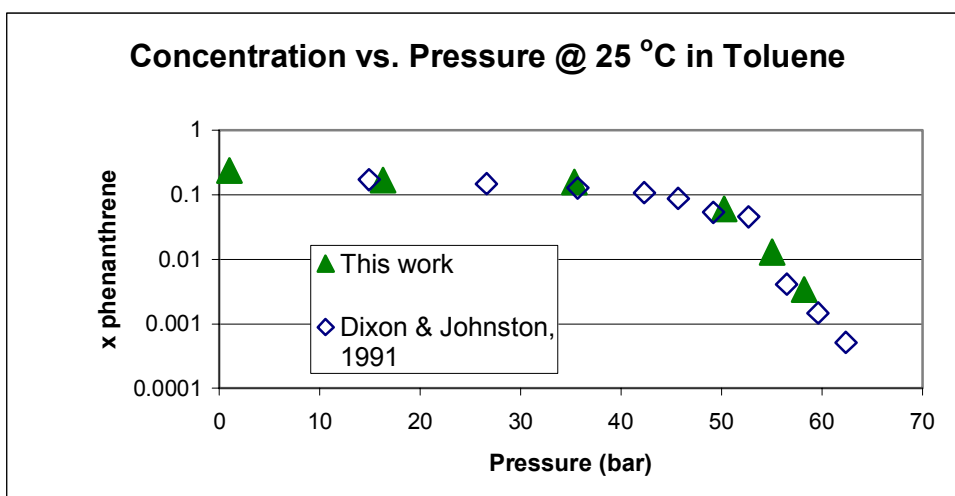


Figure 3.11: Plot of our work and the literature data from Dixon and Johnston 1991 for phenanthrene in toluene at 25 °C

This agreement from the experimental and literature data lends confidence to our method for measuring the solid solubility in antisolvent systems.

Solubility of individual solutes in ternary vs. quaternary GAS systems

Ternary systems

All the experiments took place at 25 °C. This temperature was chosen to illustrate that these separations can take place effectively without going above the critical

temperature of CO₂ (31.1 °C). Room temperature operations are also very practical for industry.

The finding in Figures 3.11 and 3.13 is congruent with Tai and Cheng, who measure the expansion/precipitation pressure of toluene with phenanthrene at 35 ± 5 bars of pressure. Tai & Cheng characterize this system as “under-saturated”. The increase of CO₂ pressure actually increases the solute/solvent mole ratio until the drop-off pressure is reached. There is a slight increase in this ratio for the toluene experiments from this thesis (Figure 3.12). In terms of the overall solubility, there seems to be a consensus from most researchers that have observed this trend that the expansion of the solvent has been said to cause the great drop in solvent power of the solution, thus a great degree of precipitation occurs {Dixon, 1991} {Mukhopadhyay, 2003} {Tai, 1998}.

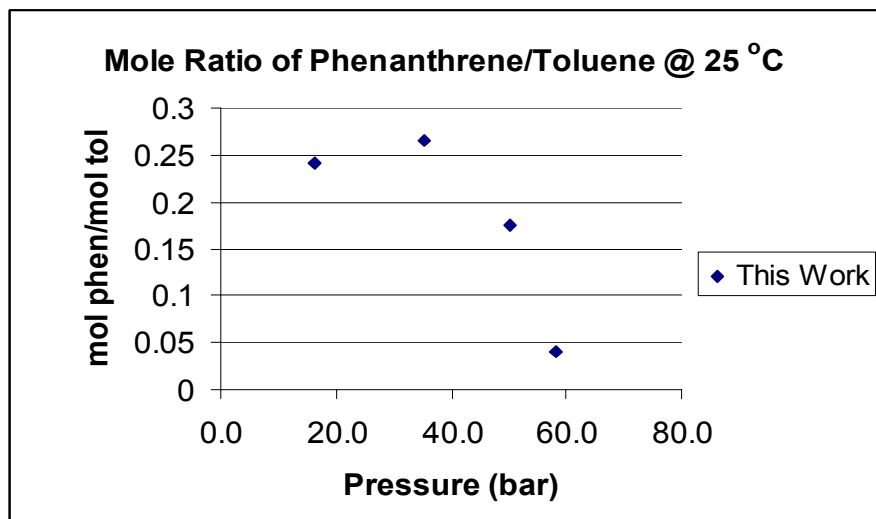


Figure 3.12: Mole fraction ratio of phenanthrene to toluene, measured in this work.

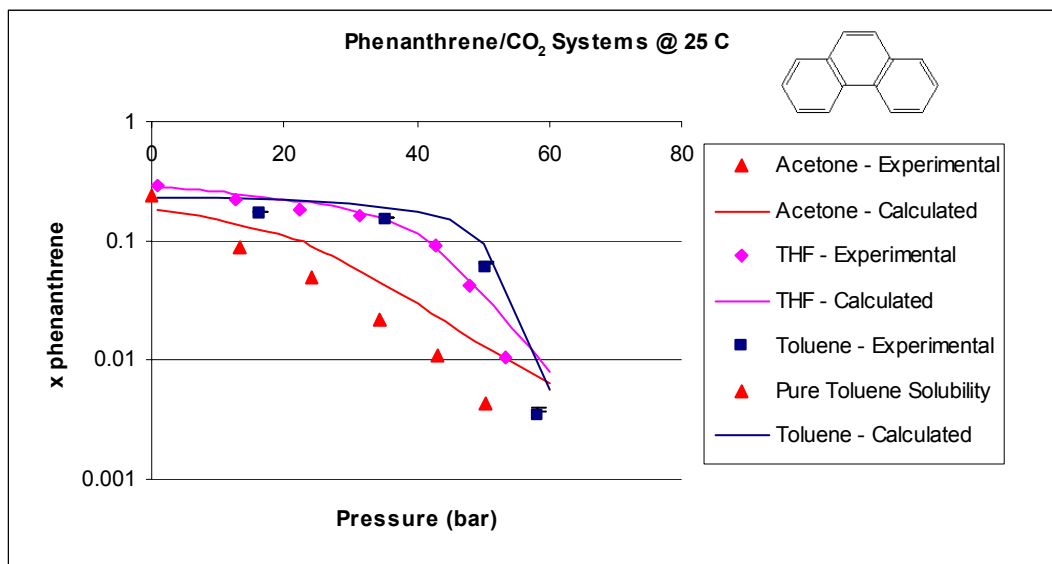


Figure 3.13: The solubility of the phenanthrene in toluene, tetrahydrofuran, and acetone with CO_2 . The calculated data is from the PRSV-HV-UNIQUAC model. All three experiments started at saturation. Tai and Cheng and measured the expansion/precipitation pressure point for the saturated toluene/phenanthrene system at 35 ± 5 bar {Tai, 1998}. All data points were taken from this work.

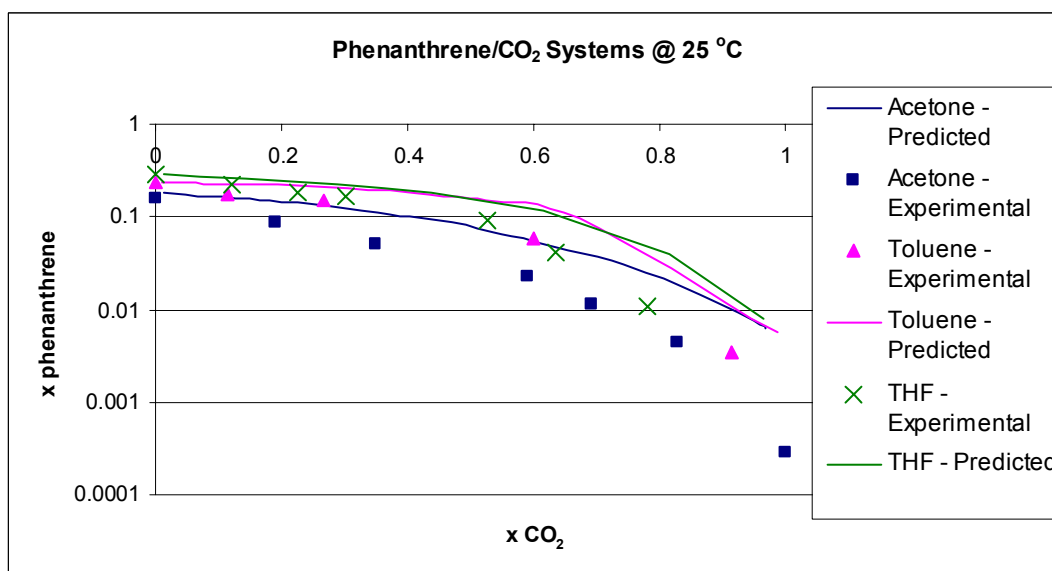


Figure 3.14: The solubility of the phenanthrene vs. the solubility of carbon dioxide in toluene, tetrahydrofuran, and acetone. The calculated data is from the PRSV-HV-UNIQUAC model. All data points were taken from this work.

The data in Figures 3.13 and 3.14 shows that PRSV-HV-UNIQUAC model predicts the overall behavior of the phenanthrene solubility well. There is some difference in the solubility at the lower pressures of approximately 30% from the predicted to the experimental values; however, the model captures the trend of solubility in the systems, including the sudden loss of phenanthrene solubility at approximately 45 bars for toluene. At this pressure, the liquid phase was observed to have expanded greatly in comparison to the expansion at the lower pressures. Very little crystal was visibly observed precipitating out of solution in the Jerguson cell until that pressure was reached.

The data for acetone and tetrahydrofuran (THF) suggest that the more soluble CO₂ is in the liquid phase, the more phenanthrene precipitates (Figure 3.14). Tetrahydrofuran had a similar solubility drop-off pressure as toluene, though not as drastic. Acetone, being the most soluble with CO₂, did not have this cliff-like solubility behavior. Rather, a steady decrease of phenanthrene concentration is observed as pressure increases. For industrial purposes, this data seems to suggest that acetone would seem to be the best solvent in terms of GXL solvent power tunability over the largest range of pressures (1 bar to approximately 60 bars at 25 °C).

Toluene would be the worst for this type of application, since there is a situation where there will be either complete precipitation or no precipitation. However, this rapid precipitation at 40 bars suggests that the crystal size will be small. The crystals will have more uniform size distribution than the acetone system. Many authors have concluded that high drastic and rapid decrease in solubility is from a high supersaturation effect, and thus, the crystals precipitate quickly and in a uniform fashion (See sources in Chapter 2).

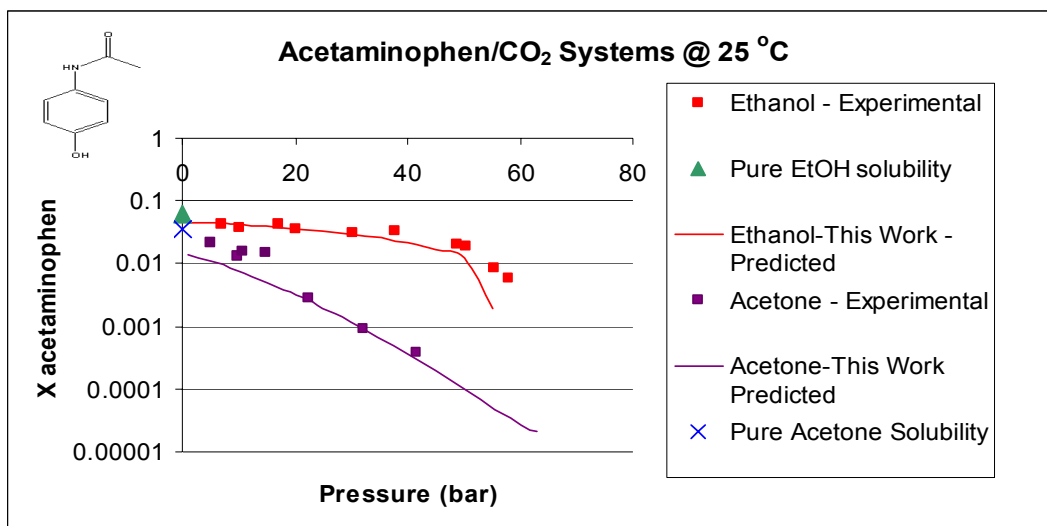


Figure 3.15: The solubility of the acetaminophen in acetone and ethanol mixtures with CO₂. The calculated data is from the PRSV-HV-UNIQUAC model. Both experiments started at saturation. The saturation concentrations were obtained from the literature {Granberg, 1999}. The other points were from this work. Tai and Cheng and measured the expansion/precipitation pressure point for the saturated ethanol/acetaminophen system at 48 ± 4 bar {Tai, 1998}.

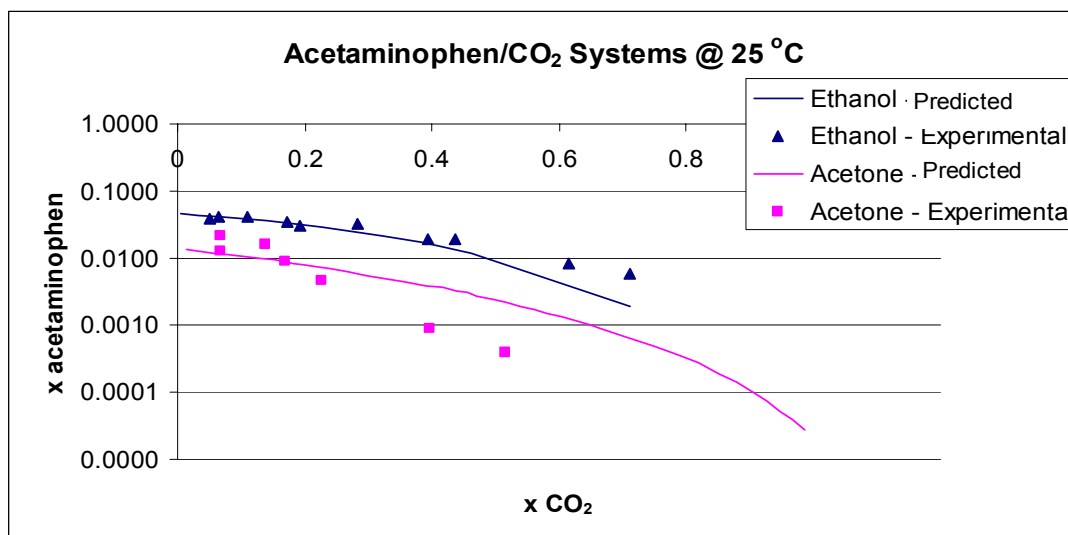


Figure 3.16: The solubility of the acetaminophen versus the solubility of carbon dioxide in acetone and ethanol. The calculated data is from the PRSV-HV-UNIQUAC model. All points from this work.

The solubility of acetaminophen is much lower than phenanthrene in most solvents (Table 3.1). Therefore, ethanol and acetone were chosen to measure solid solubility of acetaminophen.

The data in Figures 3.15 and 3.16 have a similar trend as the predicted model; however, acetone is not as good a fit as ethanol. Tai and Cheng measured the expansion/precipitation pressure of an acetaminophen/ethanol/CO₂ mixture of 48 ± 4 bars at 26 °C {Tai, 1998}. Our data has this point at approximately 50 bars, so there is good agreement with Tai and Cheng. However, there is no increase in the acetaminophen/ethanol mol ratio in the data for this thesis. Ethanol retains the acetaminophen at higher pressures due to a hydrogen bonding effect between the two components. Acetone, which is more soluble with CO₂ and has much lower hydrogen bonding than ethanol, has a steadier decrease of acetaminophen concentration as pressure increases.

Tai & Cheng classify the ethanol system as a growth system; it undergoes heterogeneous nucleation rather than bulk nucleation. Heterogeneous nucleation requires a source for the solute to aggregate towards, and this accumulation usually occurs on the walls of the vessel itself. Bulk nucleation is a crystallization that occurs throughout the entire fluid. The other systems used in this thesis were not modeled by Tai and Cheng 1998.

In all cases the solubility of CO₂ has the antisolvent effect; however, the CO₂ solubility of the solvent as well as the solute-solvent interaction(s) determine the pressure and CO₂ composition at which precipitation will occur. What we speculate as the cause of the crystallization process is that the CO₂ must penetrate the solvent shell molecules

surrounding the solute molecules. Once the composition of carbon dioxide is high enough for a particular system, the CO₂ will penetrate the solvent shell and expand the liquid, causing the decrease in solid solubility.

The PRSV-HV-UNIQUAC predicts the solid solubilities within approximately 30% at some points. However, the solubility trend was accurately predicted, including the drop-off pressure for the ethanol system. All the experimental data should be considered with approximately a maximum of 10% experimental error for pressures below 40 bar, or the solubility drop-off pressure. In the 40-65 bars range, the solubility error can get as high as 50%, due to the increased thermo-chemical sensitivity of CO₂ as it nears its critical pressure (74 bar).

Quaternary Systems

With a higher melting point, acetaminophen is not as soluble as phenanthrene in most organic liquids. However, there is the possibility of solute-solute-solvent-antisolvent interactions. Recall that such a phenomenon was found to be true to a degree in Dixon and Johnson, 1991.

The two solvents analyzed for this portion of the research were toluene and acetone.

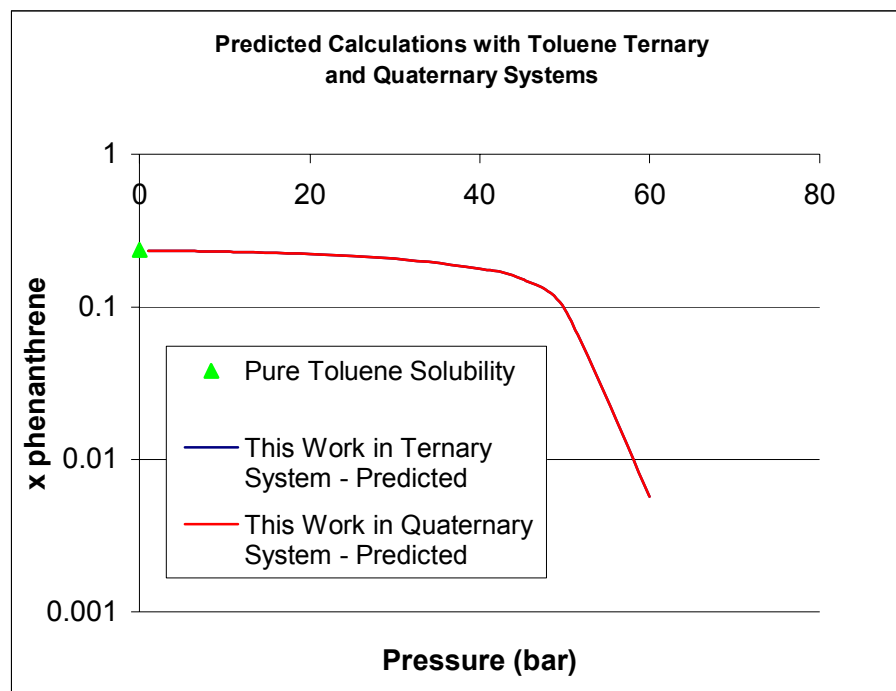


Figure 3.17: A PRSV-HV-UNIQUAC calculation of the phenanthrene concentration in a Toluene/CO₂/Phenanthrene/Acetaminophen (Quaternary) and the Toluene/CO₂/Phenanthrene (Ternary) system. The quaternary solution mole fraction was calculated using the moles of toluene, CO₂, and phenanthrene only.

Figure 3.17 illustrates that the acetaminophen will have little to no effect on the solubility. The lines are exactly on top of one another, so there is no change in concentration due to the presence of acetaminophen. Acetaminophen is only marginally soluble in toluene, 0.02% {Granberg, 1999}. Regardless, two “four component” systems were run with toluene as the solvent and yielded the results in Figure 3.18:

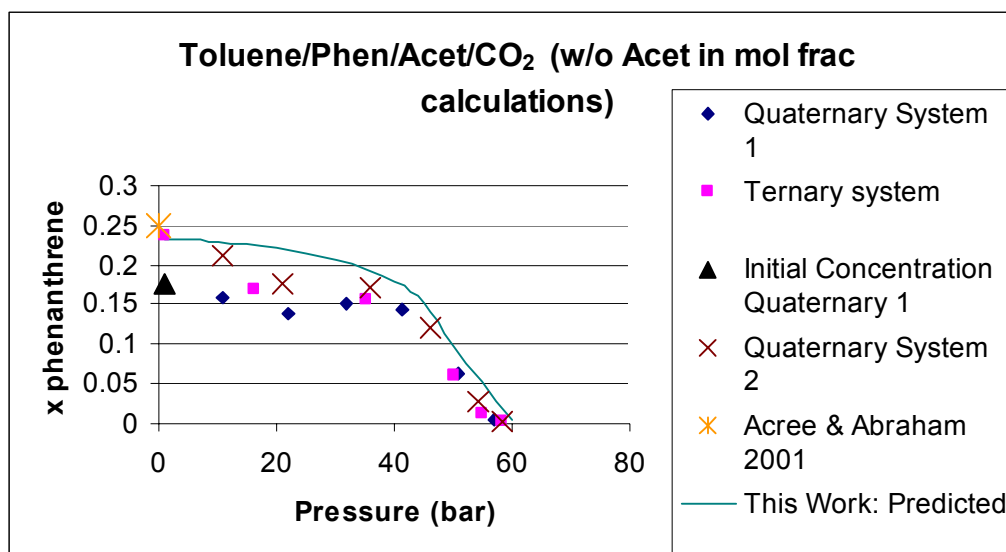


Figure 3.18: Quaternary runs of toluene/phenanthrene/acetaminophen/ CO_2 at 25 °C. The first quaternary system was done as within approximately 10% of the saturation concentration. The second quaternary system was not at saturation. These calculations were conducted using the only moles of the toluene, CO_2 , and phenanthrene. The calculated results were obtained from the PRSV-HV-UNIQUAC model.

Figure 3.18 shows that the drop-off pressure remains at 40 bars, and the experimental data follows along the predicted solubility for the higher pressures. Note the ternary behaves in nearly the exact same manner. Therefore, the presence of acetaminophen has only a marginal affect on the solubility. That is likely due to the low solubility of acetaminophen in the solvent. Acetaminophen measurements were taken, however the extremely low concentration of acetaminophen hindered the researcher from discerning the acetaminophen from the impurities in the solvents, solutes, and other sources of chemical noise in the gas chromatograph.

The presence of acetaminophen just in the solid phase does not have much effect either. The predicted solubility of both acetaminophen and phenanthrene in toluene is presented in Figure 3.19.

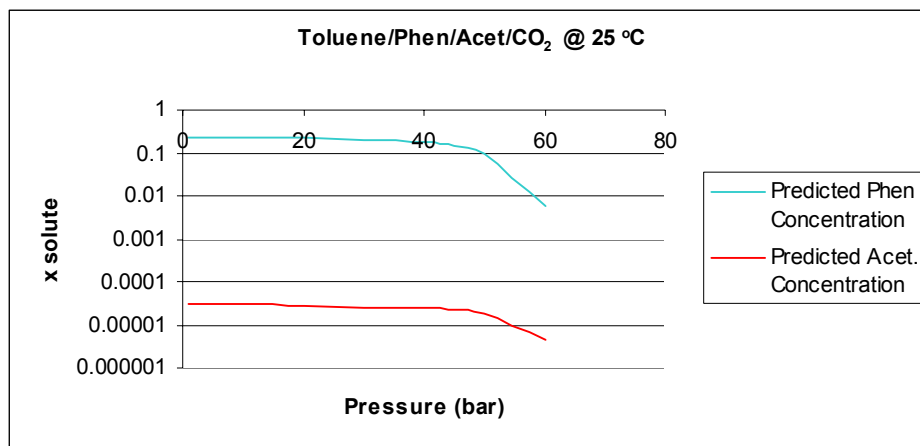


Figure 3.19: The PRSV-HV-UNIQUAC calculated solubilities of the phenanthrene and acetaminophen in a toluene/ CO_2 system.

The acetone systems are of more interest since there is solubility of each component (Figure 3.20).

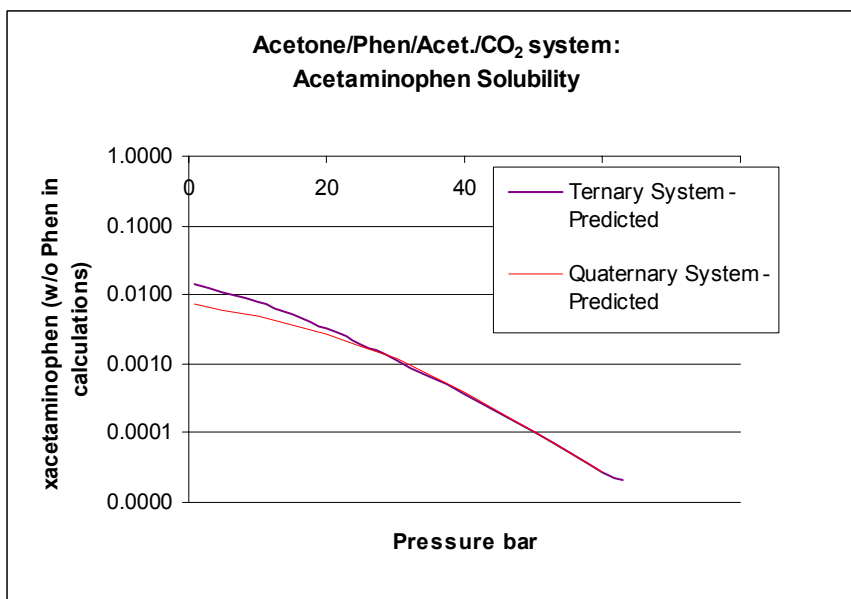


Figure 3.20: The PRSV-HV-UNIQUAC calculated solubilities of the acetaminophen/acetone in the quaternary and the ternary systems. The solubility of acetaminophen in the quaternary system was calculated using only the moles of acetone, CO_2 and the acetaminophen.

The PRSV-HV-UNIQUAC model shows that there will be a lower concentration of acetaminophen in the quaternary system up until about 27 bars of pressure. However, this model has under-predicted the solubility of acetaminophen in acetone in the ternary system, so this graph (Figure 3.20) may not be valid, even from a qualitative standpoint.

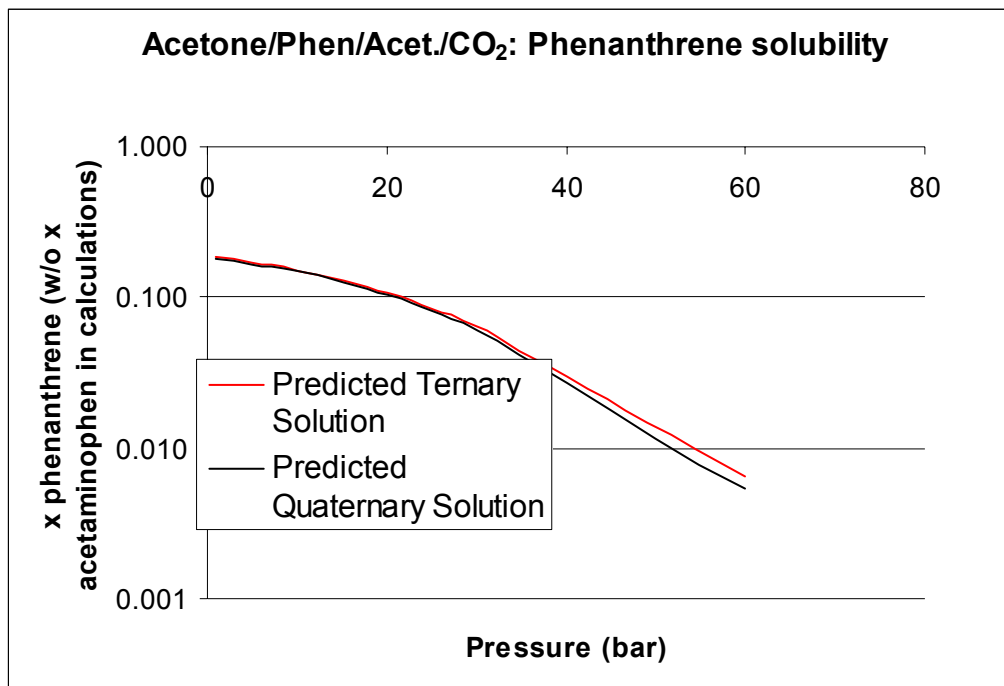


Figure 3.21: The PRSV-HV-UNIQUAC calculated solubilities of the phenanthrene/acetone in the quaternary and the ternary systems. The solubility of acetaminophen in the quaternary system was calculated using only the moles of acetone, CO_2 and the phenanthrene.

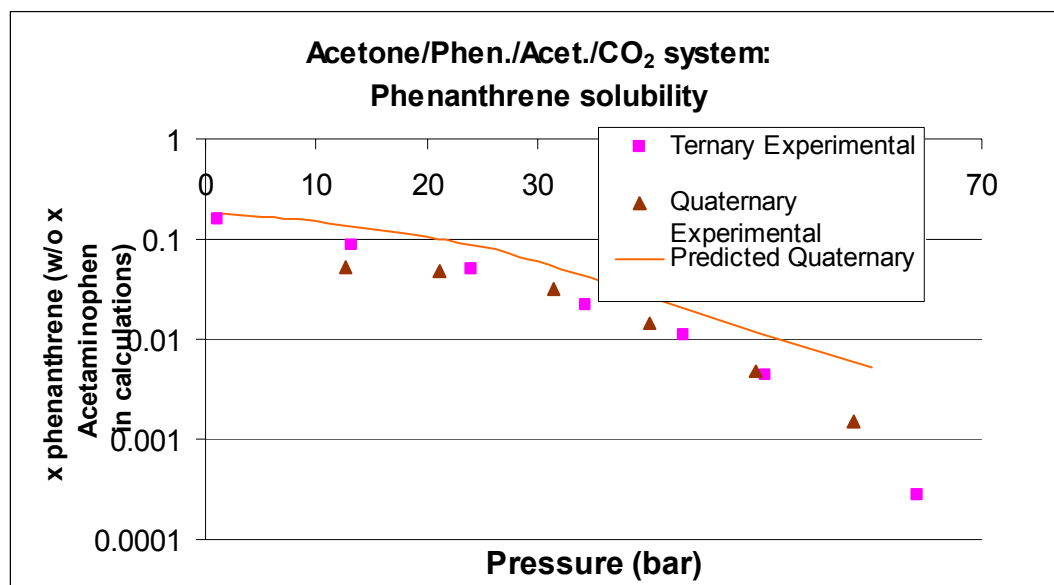


Figure 3.22: Quaternary runs of acetone/phenanthrene/acetaminophen/CO₂ at 25 °C. The quaternary system was run with a dilute solution. These calculations were conducted using the only moles of the toluene, CO₂, and phenanthrene. The calculated results were obtained from the PRSV-HV-UNIQUAC model. All points were taken from this work.

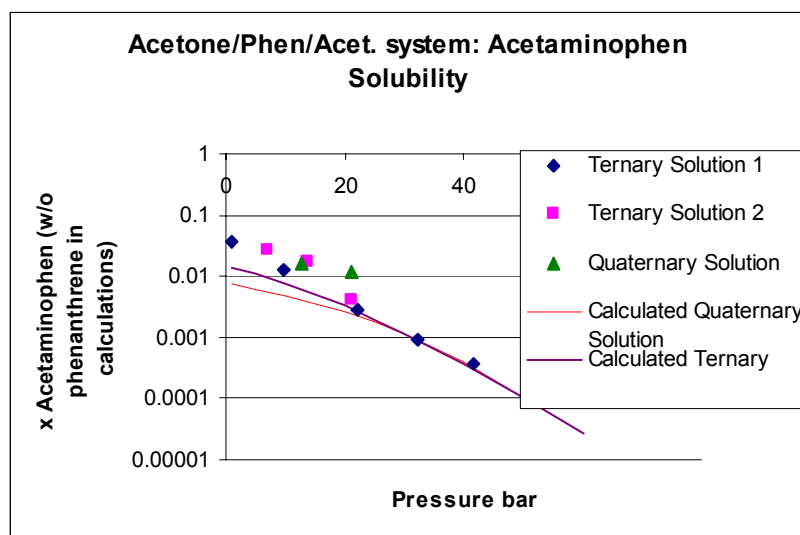


Figure 3.23: Quaternary runs of acetone/phenanthrene/acetaminophen/CO₂ at 25 °C. The first quaternary system was run with a dilute solution. These calculations were conducted using the only moles of the toluene, CO₂, and phenanthrene. The calculated results were obtained from the PRSV-HV-UNIQUAC model.

Figure 3.23 illustrates that at the higher pressure there will be up to 30% difference for solubility of phenanthrene/acetone/CO₂ in a quaternary versus the ternary system. The measured results show that the phenanthrene concentration does not change in ternary versus quaternary. The measured results make more sense because the acetaminophen does not last in the liquid solution in any appreciable amount (0.1%) past 30 bars. Secondly, the PRSV-HV-UNIQUAC does not accurately predict the actual concentration of the acetone/acetaminophen/CO₂ system. Tables of all the calculated data are in Appendix B.

There may be a slight increase in the solubility of the acetaminophen in the quaternary system, however there is a possibility that this measurement is within the margin of error. If there is an increase in the acetaminophen solubility, we speculate it would be due to the further hindrance for the CO₂ to penetrate the solvent shell surrounding acetaminophen. This increased hindrance would come from the presence of phenanthrene with solvent molecules surrounding it, which then surrounds the acetaminophen.

Conclusion

The synthetic measurement of binary phase equilibria was carried out successfully. The data for the acetone/ CO_2 and acetonitrile/ CO_2 systems matched the analytically measured results of other researchers. New binary systems were measured and matched the prediction of the Peng-Robinson equation of state with quadratic mixing rules.

The GAS analytical measurements were carried out successfully. The results were predicted using the Peng-Robinson-Stryjek-Vera equation of state with the UNIQUAC based Huron-Vidal mixing rules. The UNIQUAC parameters were set using the MOSCED model. With this equation of state and mixing rules, the solubility behavior matched the experimental data for all systems. The equation of state and mixing rules tended to over predict the solubility of the phenanthrene and under predict the solubility of acetaminophen. The phenanthrene concentration in the solvents is substantially higher than that of acetaminophen, thus the phenanthrene concentrations were probably measured with greater precision. The low solubility of acetaminophen caused a low co-solvent affect in the quaternary systems. Using the GAS method of fractional crystallization may work well, however these could be done with more appropriate examples.

CHAPTER 4

Future Recommendations

MOSCED Model

The MOSCED model seemed to yield some discrepancy for phenanthrene and paracetamol in acetone. The activity coefficient of acetaminophen in pure acetone was under-predicted by 100 percent ($\gamma_{\text{actual}} = 2.5$; $\gamma_{\text{calculated}} = 5$). Further examinations of other solutes in acetone model may need to be conducted to discover if there is a problem. Other models could also be tried for predicting solubility {Acree, 2001} {Bertucco, 1998} {Zhi-Yu, 2000} {Scurto, 2003}.

GAS Fractional Crystallization Measurements

The fractional crystallization in GXLs can prove very useful, and it has yielded useful results for other authors. Experiments can be run with isomers, diastereomers, and precursor/product molecules. All of these experiments would have industrial applications. The only hindrance would be that the melting points of molecules will have to be significantly different or the separation will not be very good.

If one were to continue to pursue GXL's use for GAS, then there must be consideration for extracting the desired product after it has come out of solution. For industrial applications, the solvent will have to be salvaged preferably without constantly compressing and decompressing the GXL. According to reviews, several researchers are working on systems similar to GAS with the subsequent separation {Thiering, 2001} {Warwick, 2000}. The same can be said for supercritical fluid processes {Jung, 2001} {Diefenbacher, 2002} {Hauthal, 2001} {Subra, 2000}. GXLs have the potential to

change the way many industries practice manufacturing, so this extraction of products should be studied further.

Furthermore, components with similar solubility in a given solvent should be analyzed to draw more conclusive findings in regards to the co-solute affect.

When conducting the experiment, it is recommended to use a uniform CO₂ addition rate. The CO₂ addition rate has been shown in the literature to greatly affect the supersaturation of a system {Dixon, 1991}. It is the speculation of this author that CO₂ addition rate also affects the time necessary for equilibrium to be fully realized.

VLE Measurements

Past research in vapor-liquid equilibria measurement using sampling and expansion volume measurements have been conducted with varying levels of success. The next step may be in-situ measurement using spectroscopy {Sala, 2004} {Marteau, 1996}. This would seemingly eliminate the possibility of taking measurements when one is not fully at equilibrium. In gas-expanded liquids, it is possible the pressure and temperature can equilibrate; however, the actual concentrations in the GXL are still changing.

APPENDIX A

APPARATUS ASSEMBLY AND PROCEDURES

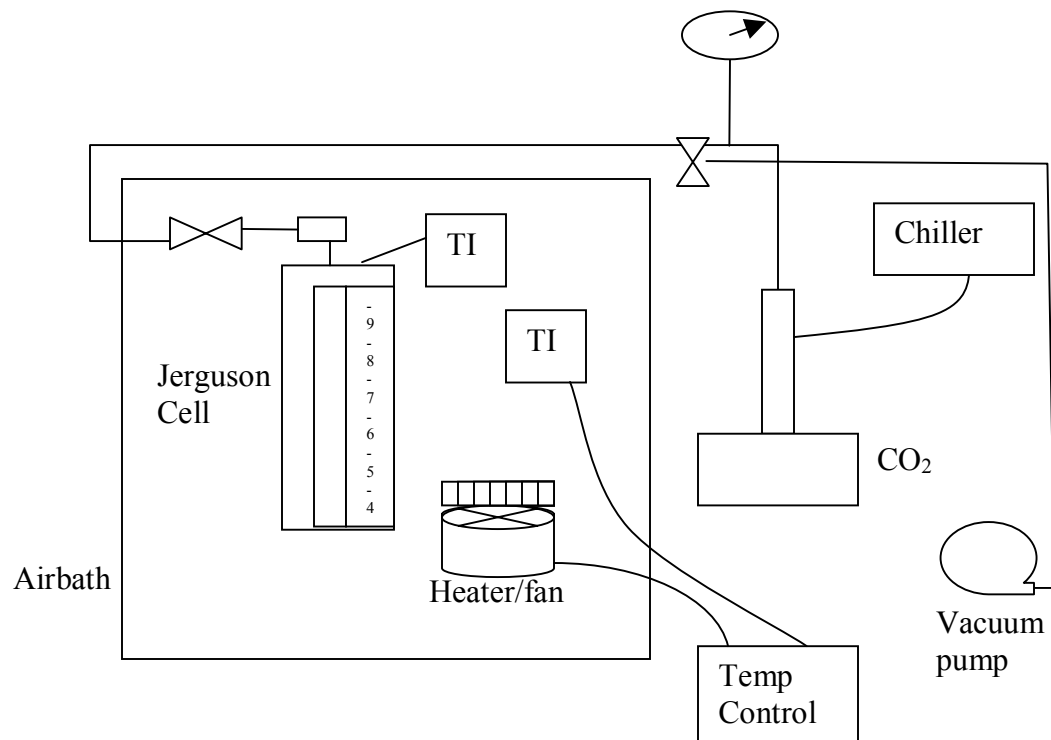


Figure A-1: Drawing of Jerguson Cell system for phase equilibria

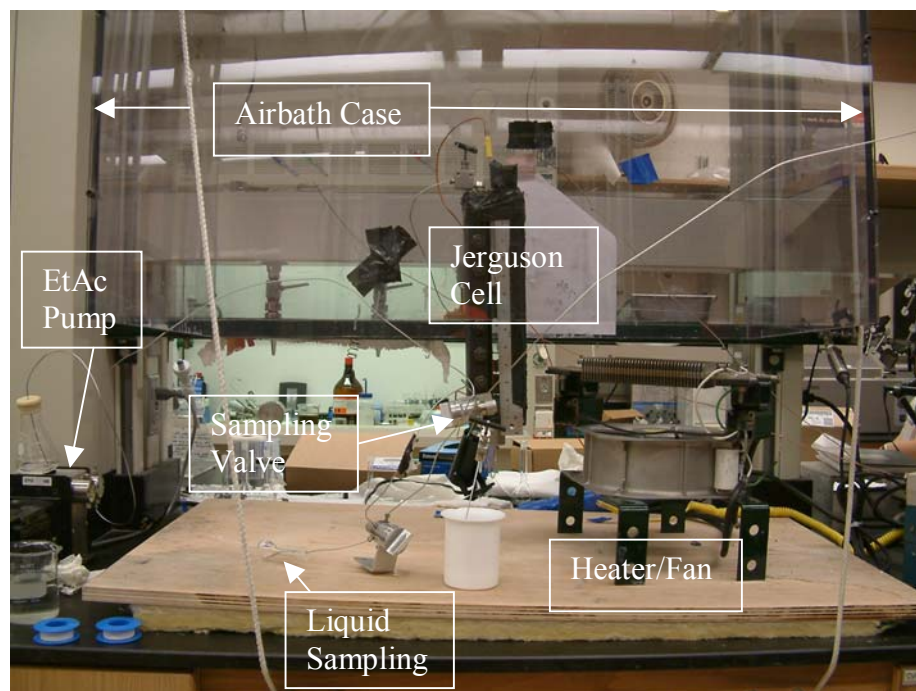


Figure A-2: Picture of Solid Solubility apparatus, Jerguson Cell, sampling valves, EtAc Pump, Heater/Fan

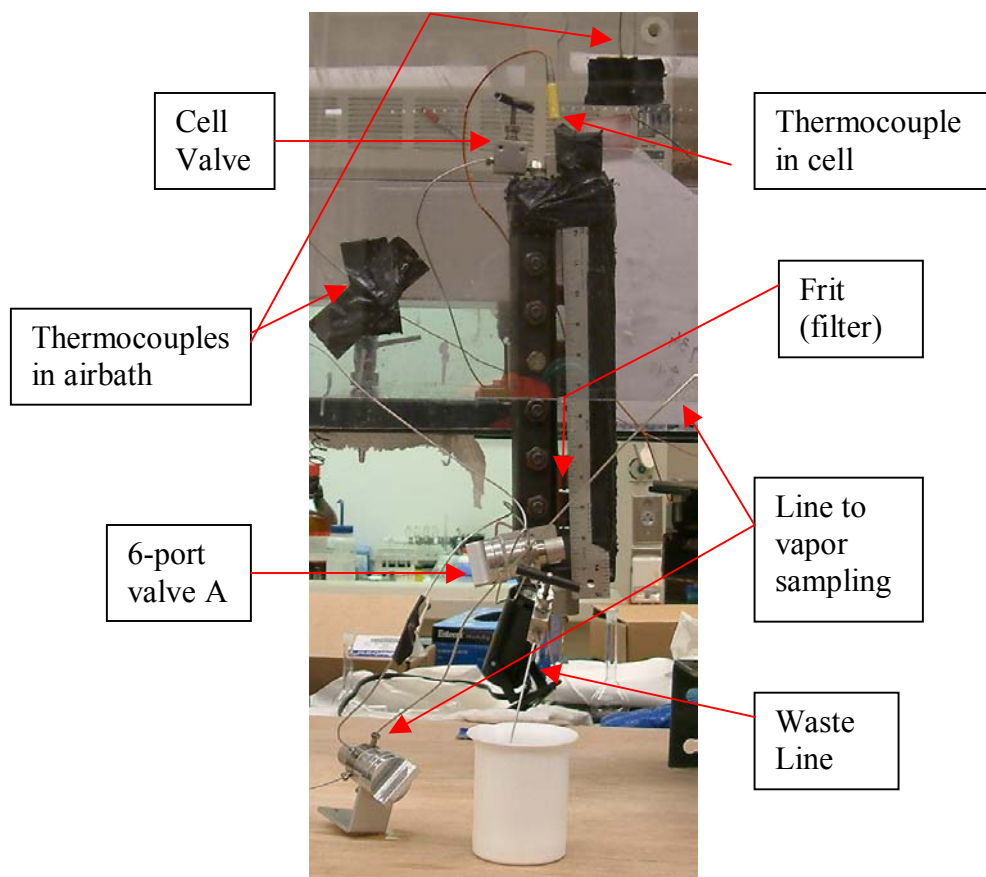


Figure A-3: Close up of Jerguson cell

Table A-1: Equipment

Name	Model #	Vendor	Information
Jerguson Cell	19-TL-10	Jerguson Gage and Valve	Visible glass length:32 cm; overall length: 38.4 cm
Airbath glass	Polycarbonate		
6-port chromatography valve	AD70076	VICI	0.4 mm fitting
Valves	15-11AF1	HiP	Called a two-way straight valve with 1.5875 mm OD
Bolts (two-port, one port)	15-21AF1N1D	HiP	Attached to top and bottom of cell respectively
ISCO	Model 500D	ISCO	Pumps CO ₂ at constant pressure and temperature.
Vacuum pump	Maxima C Plus 701585	Fisher Scientific	
Cathetometer	3921-P	Gaertner Scientific Corporation	Measure liquid level accurately
Temperature Controller	CN76000	Omega	
Digital thermometer	HH22	Omega	Displays temperature in the air bath
Digital Pressure gauge	DPI 260	Druck Inc.	
Thermocouples		Omega	
Various size HiP fittings	15-21AM1AM1	HiP	Connect lines to valves, valves to valves
Relief Valve	SS 4R3A1-BU	Swagelok	Safeguard in case pressure goes beyond relief pressure
Chiller		Endocal	Keep the ISCO at a constant temperature for phase equilibria experiments
125 mL Erlenmeyer flask			Source for EtAC pump
Gas Chromatograph	GC System HP 6890 Series	Hewlett-Packard	FID gas chromatograph
General Metal frit			filter

Apparatus assembly

The Jerguson cell is mounted using a 65 cm long pole (approximately 5 cm diameter) metal pole. The pole is attached to the back of the cell using the bolts that come with the cell. The pole is connected to two bench-top supports approximately 50 cm behind the Jerguson as shown in Figure A-4: (an adjustable pair of pliers is clamped down on the pole to allow rocking of the cell)

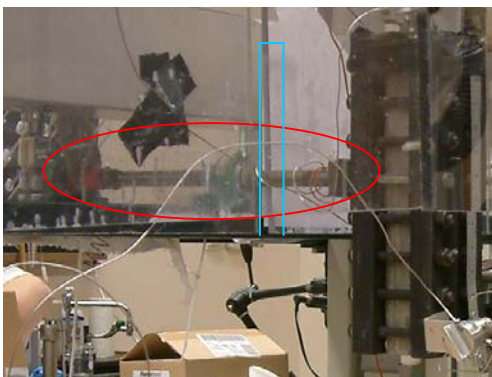


Figure A-4: Encircled: Pole connected to the Jerguson cell. This mounts the cell approximately 30 cm

The top of the cell has a two-port bolt, one opening on the top, and one on a side. A thermocouple is fit into the top of the bolt, and should go about 6 or 7 cm into the cell. The cell valve is screwed into the side port of the bolt. This valve has a stainless steel tube (0.4064-mm ID) coiled around the pole. Polycarbonate glass case must have a section cut out of the back to facilitate its raising and lowering with the support pole coming out of the back of the cell. The cell line should only go about 45 cm on the outside of the polycarbonate case until it is connected to the pressure gauge. The

pressure gauge has a short line which then goes to the relief valve. The relief valve is rated for 2,000 psig or 137 bar, which is much higher than the system operating pressures. The relief valve is connected using a male-male HiP fitting to a valve which is for the vacuum pump. This valve is connected using a male-male HiP fitting to the valve which will connect the apparatus to the ISCO. A picture of this series of valves and connections is shown below (Figure A-5):

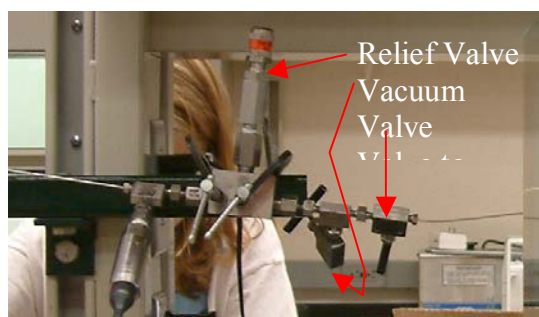
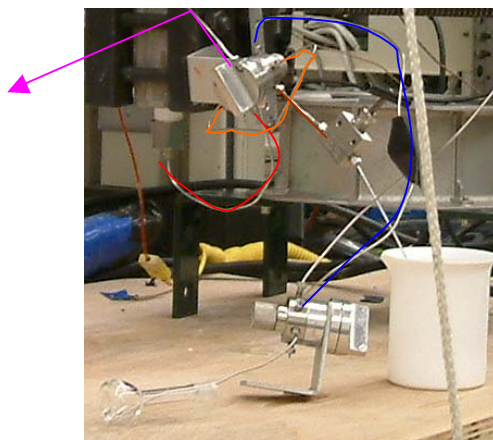


Figure A-5: The valve connections series

The ISCO is connected to a chiller using an ethylene glycol filled cooling jacket attached to the ISCO. A bolt with no external ports is screwed into the bottom of the cell (using Teflon tape) for the phase equilibria.

For the solid solubility experiments, the bolt at the bottom of the cell has a port for a line to go through it. That line is connected to a metal frit (filter) that fits inside the cell. The stainless steel line (approx. 0.15 mm ID) is connected to a mounted 6-port valve. The 6-port valve attached to the cell is explained in Figure A-6, and Figure A-7 explains how it works:



*Figure A-6: The two 6-port valves connection (all 0.15mm ID tubes) are shown and outlined in this picture with following color coding: **Line to sample**; **sample loop**; **waste/vent line**; **line to sampling valve**; **line to EtAc pump**.*

The sampling valve has two outgoing lines. Switching from one to the other will send the cell contents to a flask (liquid sampling) or an inverted buret in a water bath (vapor sampling). The water bath sampling is pictured below (Figure A-7):

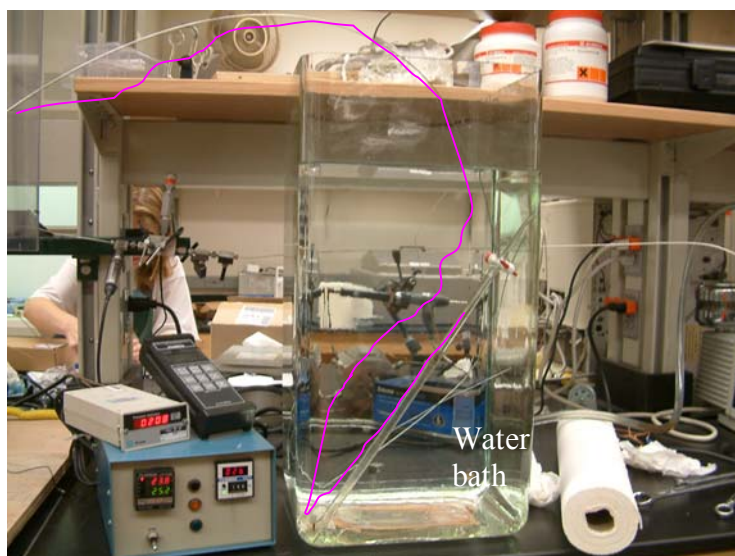


Figure A-7: The water bath with the line from the sampling 6-port valve colored.

The polycarbonate case is assembled in the dimensions 92.3925 X 91.44 X 54.61 cm³. The polycarbonate sheets are 0.635 cm thick. The case is assembled as a cube with a cut out in the back to accommodate the pole coming from the Jerguson (see Figure A-3). The actual lowering and raising of the cell is accomplished using an assembled pulley system.

Calibrations

The volume of the cell is calibrated using water put into the cell in known volume increments. The level of the water is measured using the cathetometer and pinpointing the meniscus level using the ruler attached to the cell (see Figure A-2). The cell is then emptied and cleaned out with acetone. The researcher must reattach the bolts and valves using Teflon tape wrapped around the plugs without HiP fittings. The cell is evacuated with a vacuum pump and then pressured with a known volume, and thus moles, of CO₂ from the ISCO. The researcher closes the valve from the ISCO and turns on the heater and fan to a set temperature (higher than room temperature). After the pressure in the cell stabilizes, the researcher can record the temperature and pressure, and get the volume from the literature or a reliable equation of state. The volume obtained from the CO₂ pressurization and the water level measurement will give the researcher the volumes of the liquid and vapor phases during normal experimentation.

Phase Equilibria Measurement

1. Charge the ISCO with CO₂ from a tank of pure CO₂. Set the pressure in the ISCO as well as its cooler. This will enable accurate measurement of the volume of CO₂.
 - a. The temperature of the chiller to the ISCO is set to 13.2 °C in this research. The ISCO pressure was set to 1500 psi (approx 103 bar).
2. The cell must first be cleaned out with acetone rinse and evacuated with the vacuum pump just like the calibration experiments.
 - a. The pressure gauge typically reads –7 psia during the evacuation, and continues to do so until a valve to the atmosphere, CO₂, or the full cell is opened.
3. Check that the system does not have any leaks by pressurizing the system with a few hundred pounds of CO₂ from the ISCO. The pressure in the cell should remain constant once the valve to the ISCO is closed.
 - a. If the pressure in the cell decreases, repeat step two and check for leaks again.
 - b. Bolts going directly into the cell should have their welts wrapped in Teflon tape to ensure there is no leakage. HiP fittings should fit securely in their corresponding connections.
4. Re-evacuate the system with the vacuum after this check.

- a. Note: Open a valve to the atmosphere to let the system pressure get to ambient. Vacuuming a system that is originally at high pressures could damage the vacuum pump.
5. Using a syringe with HiP fitting, close the cell valve and detach the line from said valve. Tightly screw the syringe full of the selected solvent (no air bubbles!) into the cell valve and open; the vacuum inside cell should pull the liquid into the cell to a degree.
6. Push the syringe until the desired amount of liquid is put in the cell.
7. Record the height of the liquid level, making sure there is not a significant amount of liquid sticking to the inner walls of the cell or on the supports. Rotating the cell should get most of the liquid to the base of the cell. (This could prove more difficult for very viscous liquids.)
8. Close the cell valve and connect line to the ISCO.
9. Re-evacuate the line to the ISCO **before** opening the cell valve.
10. Lower the polycarbonate airbath case making sure insulation is applied to the area around the mounting pole.
11. Open the cell valve, plug in the heater and set the temperature control to the desired temperature.
12. After temperature stabilizes, record the pressure, liquid level, temperature, and the initial volume of the carbon dioxide in the ISCO.
13. Slightly open the valve to the ISCO to let in enough CO₂ to get the desired pressure.

14. Rotate the cell using the pole sticking out of the back of the cell to mix the cell contents. Continue to do so until the pressure stops changing.
15. Repeat steps 11-14 until the desired final pressure is obtained.
16. Record the temperature, pressure, liquid height, CO₂ volume reading from the ISCO.
17. Continue to do steps 11-16 in the desired pressure increments.
 - a. This work was done with approximate increments of 10 bars (150 psia).
 - b. As you approach the critical pressure of the fluid, the expansion could go out of the top of the cell, so choose the initial liquid volume wisely.

Solid Solubility Measurements

The solubility measurements went as follows:

1. Prepare a saturated solution.
 - a. Add a certain amount of solute to the liquid.
 - b. Seal the liquid flask, and let warm water run over it for a few seconds.
 - c. If all of the solid dissolves in the warm water, add more solid.
 - d. Continue steps a-c until there is some solid left in the flask.
 - e. When charging the cell with the solution, place a few grams of the solute in the cell itself before evacuating the cell.
 - i. After this procedure, a solid phase will be visible in the cell after charging the cell, thus the solution is saturated.

- ii. A quick way to get close to saturation is to compute the saturation concentration or obtain the concentration from the literature, and use these amounts as a starting point.
2. Prepare a solution with the desired amounts of solute and solvent.
 - a. For highly concentrated solutions, solute will be lost when transferring the solution from the beaker to the syringe. Therefore it may be a good idea to weigh out the amount of solute necessary for the run, place the solid in the cell, evacuate the cell, and then add the liquid to the cell like the steps 5 and 6 in the phase equilibria measurements. This method will work best for solutions below the saturation point.
3. Charge the cell with the solution as in steps 5 and 6 from the phase equilibria measurements.
4. Make sure the sampling valve is set to rinse.
5. Lower the airbath case, and plug in the heater and set the temperature control to the desired temperature.
 - a. This work used a temperature of 25 °C, therefore it was not necessary to lower the airbath case the entire way down, since some ambient air was necessary for timely temperature control.
6. Charge the cell with the desired amount of carbon dioxide from the ISCO and rotate the cell to assist in the mixing.
 - a. Make sure the cell is steadily mixed while the CO₂ is being added, especially near the 40 bar mark. There is a possibility the solute will precipitate at the vapor-liquid boundary in the cell and make a very sturdy

plug in the middle of the cell, thus cutting off the CO₂ from the liquid mixture.

7. Attach the sampling valve to the first 6-port valve.
8. Set the sampling valve to rinse and pump ethyl acetate through the system, thus cleaning out the system.

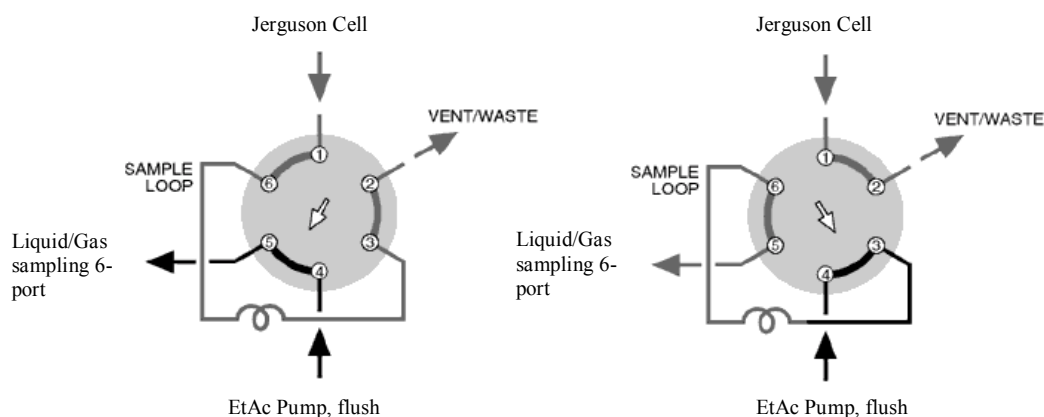


Figure A-8: A schematic of the 6-port sampling valve

9. Switch the first 6-port valve to fill the sampling loop with the cell contents. Crack open the waste valve to fill the sample loop with the cell contents.
 - a. The drawing above shows the way in which the 6-port switch works {<http://www.flowinjection.com/valves.html>}.
 - b. The waste valve should empty to a beaker of water/acetone solution. Closely observe the bubbles coming out of the waste line and a slug of ethyl acetate should be seen eventually.
 - c. Once this slug has emptied and the bubbles continue again, the sampling loop is assumed full of only the cell contents.
 - d. Close the waste valve.

10. Switch the sampling valve for liquid sampling, which should go to a 10 mL Erlenmeyer flask
11. Pump some ethyl acetate into the liquid sampling valve to the point where the opening of the line is submerged under the liquid EtAc.
12. While the EtAc is still pumping, switch the 6-port valve from sample to rinse.
The slug of the cell liquid phase will make its way to the 10 mL flask, evident by the bubbles in the flask.
 - a. A longer line to the liquid flask should be used when the pressure in the cell is very high.
 - b. A thinner line (0.0762 mm ID in this work) is recommended to decrease the chances of liquid splashing out of the flask.
 - c. For volatile solvents, the liquid sample should be collected over an ice bath.
13. Seal the flask with a cap and polyfilm tape.
14. Conduct this liquid sampling three times.
15. For vapor sampling, switch the sampling valve to the vapor sampling line. (see Figure A-8 for configuration)
16. Position the sampling vapor line to inside the inverted buret and beyond the liquid level, and record the initial water level.
 - a. When making the liquid level measurements, make sure the liquid level and the water bath level are on the same plane to decrease error from pressure differences.

17. Sample the vapor in the exact same manner as the liquid level, recording the final liquid level in the buret.
 - a. If more than 2 mL of EtAc is in the buret, record the levels of the EtAc and the water in the buret and adjust for density differences.
18. This difference in vapor volume is the amount of CO₂ in the sample. Conduct this sampling three times.
19. Load the liquid samples in the gas chromatograph. The output of the GC should correspond with the fit from the calibration curve.

APPENDIX B
EXPERIMENTAL DATA

Phase Equilibria Data

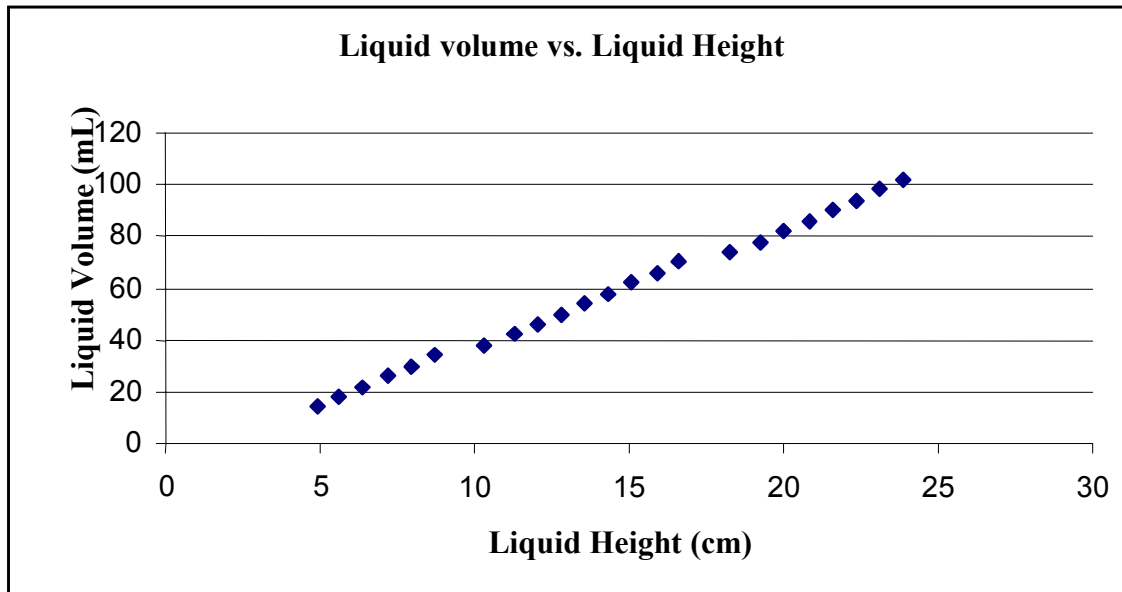


Figure B-1: Jerguson Cell Volume Calibration

Figure B-1 shows the calibration of the Jerguson cell for the Binary VLE portion of the thesis. The inconsistency in the calibration chart comes from the horizontal supports inside the cell. These supports provide a partial block inside the cell and facilitate more effective mixing when rocking the cell back and forth. The meniscus is visible yet difficult to measure when the fluid is at the level of the supports, so the liquid level is measured above and below the supports. During experimentation, if the GXL liquid level was at the supports, the liquid level height was measured as accurately as

possible and a linear interpolation of the above and below calibration points were used to estimate the liquid volume.

Table B-1: Jerguson Cell Volume Calibration Values. Water volume height measured using an attached ruler on the Jerguson Cell with the fine measurement from the cathetometer

Volume	height				
mL	whole in.	/16 in	add. cm	height (cm)	Vol (ml)
14	1	15	0	4.921	14
18	2	3	0.0544	5.610	18
22	2	8	0.0395	6.39	22
26	2	13	0.0583	7.20	26
30	3	2	0	7.94	30
34	3	7	0	8.73	34
38	4	1	0	10.3	38
42	4	7	0.015	11.3	42
46	4	12	0	12.1	46
50	5	0	0.1165	12.8	50
54	5	5	0.0946	13.6	54
58	5	10	0.064	14.4	58
62	5	15	0.0295	15.1	62
66	6	4	0.0533	15.9	66
70	6	8	0.0979	16.6	70
74	7	3	0	18.3	74
78	7	9	0.0395	19.2	78
82	7	14	0	20.0	82
86	8	3	0	20.8	86
90	8	8	0	21.6	90
94	8	12	0.0955	22.3	94
98	9	1	0.0645	23.1	98
102	9	6	0.058	23.9	102

Table B-2: Expansion Data of N-methyl-pyrrolidone at 40 °C

P /psia	P bar	Vol.	% Vol
0	0	21.1	0
104	7.07	21.5	0.0200
224	15.2	22.7	0.074
299	20.3	23.6	0.117
408	27.8	24.8	0.176
511	34.8	26.2	0.240
607	41.3	28.2	0.334
709	48.2	30.2	0.429
812	55.2	33.2	0.570
906	61.6	36.4	0.725
1007	68.5	44.6	1.11
1128	76.7	62.7	1.97

Table B-3: Expansion data of Dichloromethane at 40 °C

P /psia	P bar	Vol.	% Vol
17	1.16	16.9	0
80	5.44	19.3	0.142
180	12.2	20.3	0.197
279	18.98	21.9	0.291
382	26.0	24.0	0.417
582	39.6	30.1	0.779
675	45.9	32.3	0.910
774	52.7	46.1	1.72
873	59.4	59.3	2.50
969	65.9	92.5	4.46
1008	68.6	120.	5.20

Table B-4: Expansion data for Acetone at 40 °C

P /psia	P bar	Vol.	% Vol
8	0.544	16.1	0
106	7.21	17.3	0.0737
304	20. 7	20.2	0.253
412	28.0	22.6	0.400
507	34.5	25. 7	0.590
632	43.0	30. 7	0.900
737	50.1	37.2	1.30
833	56. 7	47.1	1.92
917	62.4	61.4	2.78
1004	68.3	89.4	4.54

Table B-5: Expansion data for Tetrahydrofuran at 40 °C

P /psia	P bar	Vol.	% Vol
4	0.272	19.8	0
84	5.71	20.4	0.0283
165	11.2	21.5	0.0840
229	15.6	22.5	0.133
285	19.4	24.0	0.210
362	24.6	25.4	0.281
449	30.5	28.1	0.417
522	35.5	30.3	0.529
594	40.4	33.7	0.700
663	45.1	37.3	0.882
745	50. 7	44.3	1.23
803	54.6	50.6	1.55
881	59.9	61.4	2.10

Table B-6: Expansion data for Nitromethane at 40 °C

P /psia	P bar	Vol.	% Vol
		22.4	0
72	4.90	24.0	0.0700
180	12.2	25.2	0.126
278	18.9	26.5	0.183
388	26.4	28.7	0.281
482	32.8	31.1	0.388
579	39.4	34.0	0.518
711	48.4	40.2	0.794
800	54.4	45.6	1.04
893	60.7	53.7	1.40
984	66.9	71.1	2.18
1040	70.7	94.8	3.23

Table B-7: Expansion data for Acetonitrile at 40 °C

P /psia	P bar	Vol.	% Vol
		29.8	0
81	5.510	31.0	0.0387
154	10.5	32.7	0.0936
262	17.8	35.4	0.185
360	24.5	39.2	0.315
439	29.9	42.5	0.425
550	37.4	47.7	0.599
653	44.4	53.8	0.804
749	51.0	63.0	1.11
826	56.2	73.4	1.46
908	61.8	93.0	2.12

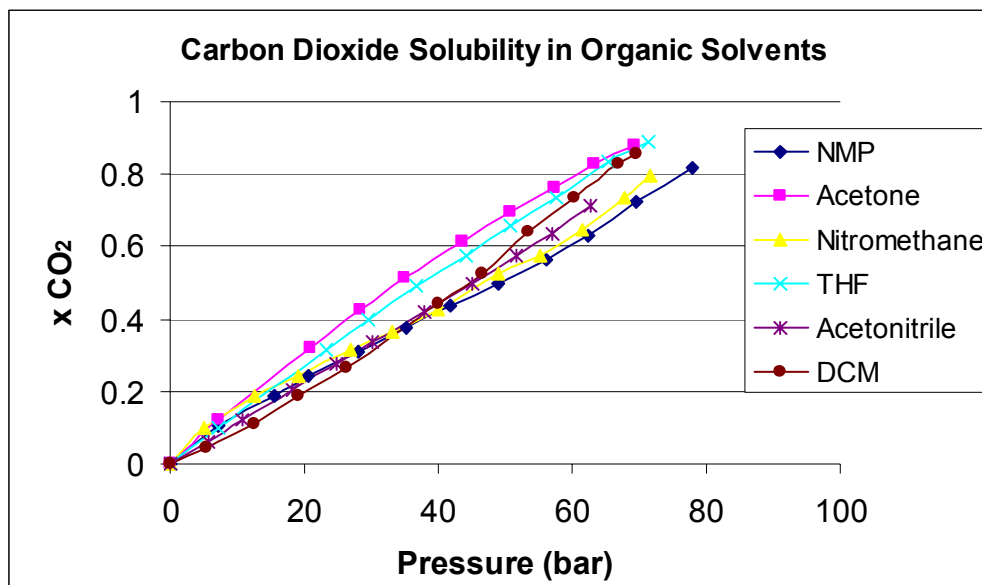


Figure B-2: Solubility of carbon dioxide vs. Pressure for the various solvents used in this thesis

The following tables illustrate the difference between the experimental mole fraction and the calculated mole fraction at the same pressure. The same equation of state was used in the calculation of the experimental mole fraction; however, the EOS was only used in the calculation of the vapor phase composition and density. The vapor phase is about 98% carbon dioxide at all pressures above 5 bar, therefore neither the equation of state or the binary interaction parameter have an appreciable affect on the final value of the experimental liquid phase composition.

Table B-8: CO_2 (1) and Acetone (2) Binary mixture at 40 °C

	Experimental		Calculated		Difference
Pressure (bar)	x1	x2	x1	x2	x2exp-x2calc
0.563	0.000	1.000	0.000	1.000	0.000
7.310	0.120	0.880	0.104	0.896	-0.016
20.966	0.321	0.679	0.301	0.699	-0.019
28.414	0.423	0.577	0.402	0.598	-0.021
34.966	0.515	0.485	0.486	0.514	-0.029
43.586	0.615	0.385	0.593	0.407	-0.022
50.828	0.695	0.305	0.678	0.322	-0.017
57.448	0.763	0.237	0.753	0.247	-0.010
63.241	0.827	0.173	0.815	0.185	-0.012
69.241	0.879	0.121	0.876	0.124	-0.003

Table B-9: CO_2 (1) and Nitromethane (2) Binary mixture at 40 °C

	Experimental		Calculated		Difference
Pressure (bar)	x1	x2	x1	x2	x2exp-x2calc
0.105	0.000	1.000	0.000	1.000	0.000
4.966	0.100	0.900	0.056	0.944	-0.044
12.414	0.190	0.810	0.141	0.859	-0.049
19.172	0.242	0.758	0.217	0.783	-0.025
26.759	0.313	0.687	0.300	0.700	-0.013
33.241	0.365	0.635	0.370	0.630	0.005
39.931	0.426	0.574	0.441	0.559	0.015
49.034	0.523	0.477	0.536	0.464	0.013
55.172	0.572	0.428	0.599	0.401	0.027
61.586	0.647	0.353	0.666	0.334	0.018
67.862	0.737	0.263	0.732	0.268	-0.005
71.724	0.794	0.206	0.776	0.224	-0.019

Table B-10: CO₂ (1) and Tetrahydrofuran (2) Binary mixture at 40 °C

	Experimental		Calculated		Difference
Pressure (bar)	x1	x2	x1	x2	x2exp-x2calc
0.423	0.000	1.000	0.000	1.000	0.000
7.103	0.098	0.902	0.095	0.905	-0.003
23.241	0.313	0.687	0.312	0.688	-0.002
29.655	0.398	0.602	0.394	0.606	-0.005
36.828	0.489	0.511	0.483	0.517	-0.006
44.207	0.576	0.424	0.573	0.427	-0.003
50.690	0.655	0.345	0.651	0.349	-0.004
57.517	0.733	0.267	0.732	0.268	-0.001
65.241	0.832	0.168	0.821	0.179	-0.010
71.379	0.890	0.110	0.888	0.112	-0.002

Table B-11: CO₂ (1) and Dichloromethane (2) Binary mixture at 40 °C

	Experimental		Calculated		Difference
Pressure (bar)	x1	x2	x1	x2	x2exp-x2calc
1.024	0.000	1.000	0.000	1.000	0.000
5.517	0.044	0.956	0.049	0.951	0.005
12.414	0.112	0.888	0.124	0.876	0.012
19.241	0.185	0.815	0.200	0.800	0.015
26.345	0.266	0.734	0.281	0.719	0.015
40.138	0.440	0.560	0.449	0.551	0.009
46.552	0.524	0.476	0.533	0.467	0.009
53.379	0.641	0.359	0.629	0.371	-0.012
60.207	0.736	0.264	0.730	0.270	-0.006
66.828	0.828	0.172	0.826	0.174	-0.002
69.517	0.857	0.143	0.862	0.138	0.005

Table B-12: CO₂ (1) and Acetonitrile (2) Binary mixture at 40 °C

Pressure (bar)	Experimental		Calculated		Difference
	x1	x2	x1	x2	x2exp-x2calc
0.213	0.000	1.000	0.000	1.000	0.000
5.586	0.063	0.937	0.055	0.951	-0.014
10.621	0.123	0.877	0.107	0.899	-0.022
18.069	0.204	0.796	0.186	0.797	-0.001
24.828	0.278	0.722	0.254	0.745	-0.024
30.276	0.339	0.661	0.310	0.693	-0.032
37.931	0.421	0.579	0.383	0.640	-0.061
45.034	0.499	0.501	0.451	0.586	-0.085
51.655	0.573	0.427	0.540	0.471	-0.045
56.966	0.638	0.362	0.644	0.339	0.023
62.621	0.711	0.289	0.728	0.261	0.028

Table B-13: MOSCED Parameters for every component used in this thesis

Solute	v	lambda	tau	q	alpha	beta
CO ₂	55	11	6.1	0.8	2.6	1.4
acetonitrile	52.2	16.03	11.83	1	2.57	9.45
acetone	74.4	15.83	8.55	1	0	11.14
dichloromethane	64.1	17.57	5.77	0.96	4.07	1.06
N-methylpyrrolidone	76.83	19.71	8.44	1	0	23.92
tetrahydrofuran	81.1	17.14	4.22	1	0	9.98
nitromethane	53.7	18.92	12.08	1	4.64	4.06
ethyl acetate	97.8	16.45	5.82	1	0	7.85
ethanol	58.4	15.5	2.83	1	12.33	13.63
paracetamol	120	18.9	0.24	0.9	16.5	12.66
phenanthrene	167.077	19.41	5.13	0.9	0	0.84
toluene	106.3	17.96	2.52	0.9	0.84	2.41

Table B-13 exhibits the current MOSCED parameters for every molecule used in this thesis. The Binary VLE components are presented here to show the likeness in the parameters for CO₂ and the other solvents. Using the MOSCED parameters one can

observe the affects of hydrogen bonding (α, β parameters), polarity (λ), dipolarity (τ), and size difference (ν) on solubility.

Fractional Crystallization Data

Gas chromatograph calibrations for the components are presented below. All the components were dissolved in ethyl acetate to measure the area response, since ethyl acetate was the rinsing fluid. The concentration is in mg of solute per ml of ethyl acetate.

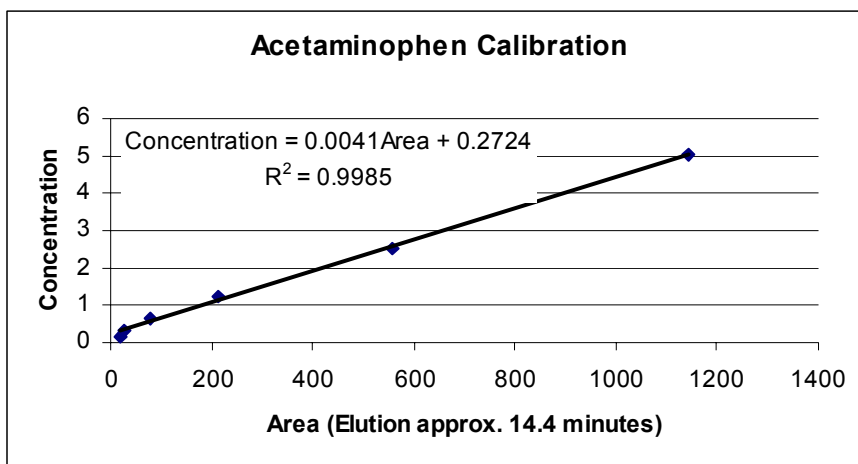


Figure B-3: Gas chromatograph calibration of acetaminophen in ethyl acetate

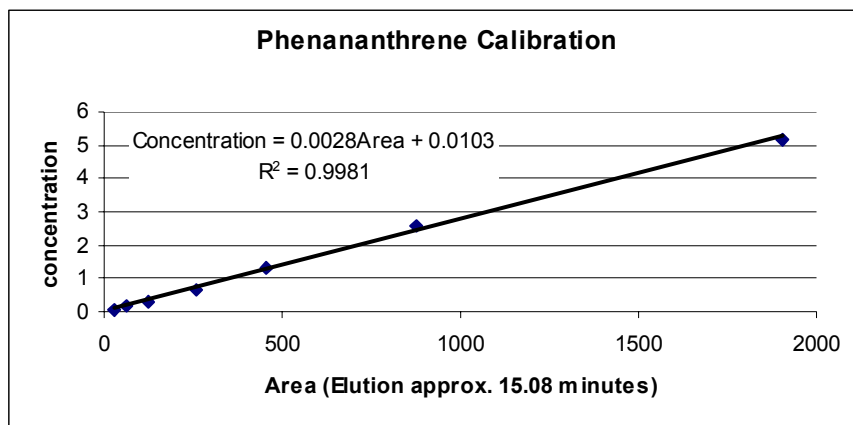


Figure B-4: Gas chromatograph calibration of phenanthrene in ethyl acetate

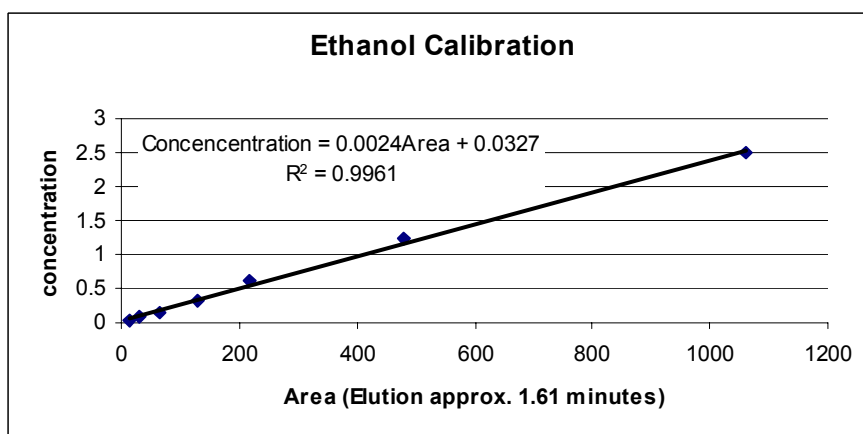


Figure B-5: Gas chromatograph calibration of ethanol in ethyl acetate

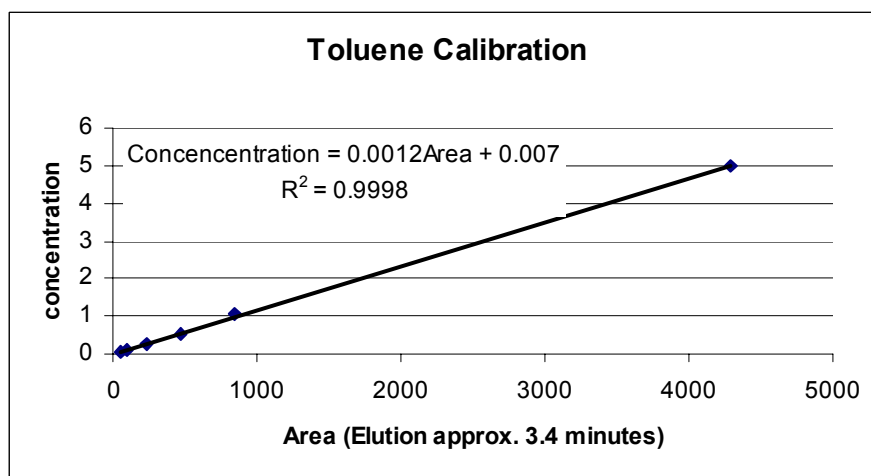


Figure B-6: Gas chromatograph calibration of toluene in ethyl acetate

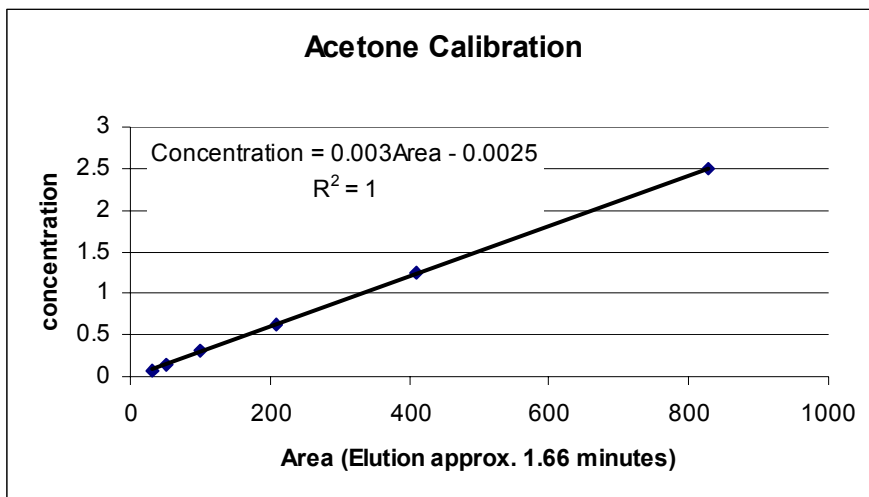


Figure B-7: Gas chromatograph calibration of acetone in ethyl acetate

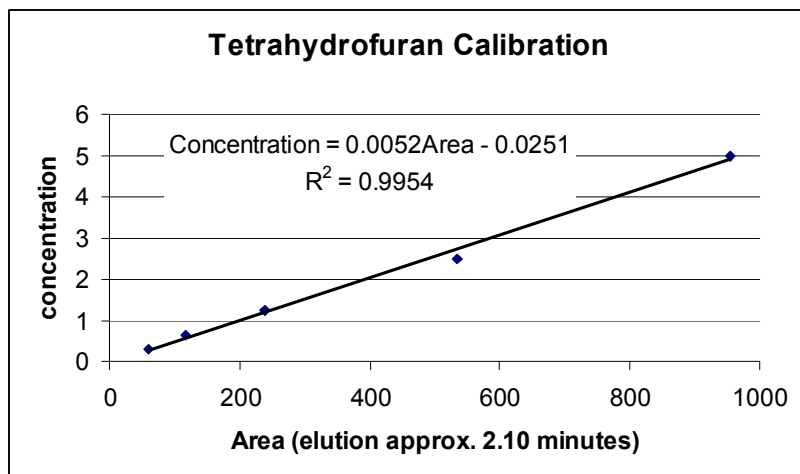


Figure B-8: Gas chromatograph calibration of tetrahydrofuran in ethyl acetate.

Presented below are the experimental and predicted mole fractions of the ternary and quaternary systems. The UNIQUAC interaction parameter matrix is also presented for each system.

Table B-14: Experimental Mole fractions and pressures for Toluene/Phenanthrene/CO₂ system at 25 °C

Experimental Values			
	CO ₂	Toluene	Phenanthrene
Pressure (bar)	x1	x2	x3
0	0.000	0.763	0.237
16.3	0.116	0.712	0.172
35.4	0.267	0.579	0.153
50.3	0.600	0.340	0.060
58.2	0.913	0.084	0.003

Table B-15: PRSV-HV-UNIQUAC predicted concentrations for Toluene/Phenanthrene/CO₂ system at 25 °C

Predicted Values			
	CO ₂	Toluene	Phenanthrene
Pressure (bar)	x1	x2	x3
1	0.00878	0.758	0.233
2.5	0.02244	0.746	0.233
5	0.04549	0.722	0.232
10	0.09271	0.677	0.23
20	0.19273	0.585	0.222
30	0.30367	0.489	0.207
40	0.43651	0.385	0.178
45	0.52354	0.324	0.152
50	0.67256	0.231	0.0960
60	0.98801	0.00630	0.00569

Table B-16: UNIQUAC interaction parameter matrix Toluene/Phenanthrene/CO₂

u _{ij}	CO ₂	Toluene	Phenanthrene
CO ₂	0	179.1796976	349.7386
Toluene	604.5463403	0	128.3496
Phenanthrene	756.1666039	-72.43374906	0

Table B-17: Experimental Mole fractions and pressures for Tetrahydrofuran/Phenanthrene/CO₂ system at 25 °C

Experimental Values			
	CO ₂	Tetrahydrofuran	Phenanthrene
Pressure (bar)	x1	x2	x3
0	0	0.7116	0.2884
12.6	0.122	0.652	0.226
22.3	0.225	0.590	0.186
31.4	0.301	0.536	0.163
42.8	0.526	0.384	0.090
47.9	0.634	0.324	0.041
53.3	0.780	0.210	0.011

Table B-18: PRSV-HV-UNIQUAC predicted concentrations for Tetrahydrofuran/Phenanthrene/CO₂ system at 25 °C

Predicted Values			
	CO ₂	Tetrahydrofuran	Phenanthrene
Pressure (bar)	x1	x2	x3
1	0.012	0.705	0.283
5	0.070	0.657	0.273
10	0.143	0.599	0.259
20	0.288	0.488	0.225
25	0.362	0.434	0.204
30	0.439	0.381	0.180
40	0.616	0.269	0.115
49	0.817	0.143	0.040
60	0.966	0.026	0.008

Table B-19: UNIQUAC interaction parameter matrix for Tetrahydrofuran/Phenanthrene/CO₂

u _{ij}	CO ₂	tetrahydrofuran	Phenanthrene
CO ₂	0	27.08147821	271.9483225
Tetrahydrofuran	235.7201443	0	-447.1850534
Phenanthrene	560.4750884	624.7433131	0

Table B-20: Experimental Mole fractions and pressures for Acetone/Phenanthrene/CO₂ system at 25 °C

Experimental Values			
	CO ₂	Acetone	Phenanthrene
Pressure (bar)	x1	x2	x3
0	0	0.840	0.160
13.2	0.189	0.722	0.089
24.0	0.350	0.600	0.050
34.3	0.591	0.387	0.022
43.2	0.691	0.297	0.011
50.6	0.830	0.166	0.004

Table B-21: PRSV-HV-UNIQUAC predicted concentrations for Acetone/Phenanthrene/CO₂ system at 25 °C

Predicted Values			
Pressure (bar)	CO ₂	Acetone	Phenanthrene
	x1	x2	x3
1	0.013	0.803	0.184
5	0.087	0.742	0.171
10	0.180	0.668	0.152
20	0.371	0.521	0.109
25	0.469	0.446	0.085
30	0.566	0.371	0.063
40	0.742	0.228	0.030
49	0.864	0.121	0.015
60	0.968	0.025	0.006

Table B-22: UNIQUAC interaction parameter matrix for Acetone/Phenanthrene/CO₂

u _{ij}	CO ₂	Acetone	Phenanthrene
CO ₂	0	-176.3879	271.9483
Acetone	369.9978	0	-217.7871
Phenanthrene	560.4751	332.3661	0

Table B-23: Experimental Mole fractions and pressures for Acetone/Acetaminophen/CO₂ system at 25 °C

Experimental Values			
	CO ₂	Acetone	Acetaminophen
Pressure (bar)	x1	x2	x3
0.0	0.000	0.964	0.036
6.89	.074	.898	.028
9.8	0.067	0.920	0.013
13.9	.187	.794	.0185
21.0	.341	.646	.0123
22.1	0.226	0.769	0.00475
31.7	.504	.484	.0118
31.9	0.397	0.596	0.000901
41.1	.701	.299	0
41.3	0.517	0.482	0
48.6	0.766	0.234	0
49.6	.939	.061	0
57.0	0.852	0.148	0

Table B-24: PRSV-HV-UNIQUAC predicted concentrations for Acetone/Acetaminophen/CO₂ system at 25 °C

Predicted Values			
	CO ₂	Acetone	Acetaminophen
Pressure (bar)	x1	x2	x3
1	0.015	0.971	0.0138
5	0.105	0.884	0.0108
10	0.218	0.774	0.00756
20	0.438	0.558	0.00320
25	0.539	0.459	0.00195
30	0.631	0.367	0.00115
40	0.786	0.213	0.000358
50	0.904	0.0957	0.000101
60	0.988	0.0120	0.0000272

Table B-25: UNIQUAC interaction parameter matrix for Acetone/Acetaminophen/CO₂

u _{ij}	CO ₂	Acetone	Acetaminophen
CO ₂	0	-176.39	724.865
Acetone	369.998	0	30.758
Acetaminophen	899.927	259.539	0

Table B-26: Experimental Mole fractions and pressures for Ethanol/Acetaminophen/CO₂ system at 25 °C

Experimental Values			
	CO ₂	Ethanol	Acetaminophen
Pressure (bar)	x1	x2	x3
1	0	0.763	0.237
6.90	0.0650	0.893	0.0415
9.93	0.0519	0.909	0.0387
16.9	0.109	0.849	0.0416
20.2	0.174	0.791	0.0348
30.3	0.194	0.775	0.0313
37.8	0.283	0.684	0.0328
48.8	0.394	0.586	0.0197
50.1	0.438	0.543	0.0195
55.4	0.614	0.377	0.00839
57.8	0.711	0.283	0.00589

Table B-27: PRSV-HV-UNIQUAC predicted concentrations for Ethanol/Acetaminophen/CO₂ system at 25 °C

Predicted Values			
	CO ₂	Ethanol	Acetaminophen
Pressure (bar)	x1	x2	x3
1	0.00624	0.947	0.0465
5	0.0336	0.922	0.0445
10	0.0687	0.889	0.0418
20	0.143	0.821	0.0359
30	0.226	0.745	0.0293
40	0.324	0.654	0.0217
45	0.384	0.598	0.0172
50	0.464	0.524	0.0120
55	0.713	0.285	0.00192

Table B-28: UNIQUAC interaction parameter matrix for Ethanol/Acetaminophen/CO₂

u _{ij}	CO ₂	Ethanol	Acetaminophen
CO ₂	0	722.015	927.4981199
Ethanol	239.127	0	-49.05386884
Acetaminophen	967.435	202.791	0

Table B-29: Experimental Mole fractions and pressures for Toluene/Acetaminophen/Phenanthrene/CO₂ system at 25 °C

Experimental Values				
	CO ₂	Toluene	Acetaminophen	Phenanthrene
Pressure (bar)	x1	x2	x3	x4
First Run				
0	0	0.749	0	0.251
10.7	0.130	0.658	0	0.211
21.0	0.157	0.664	0	0.179
36.1	0.303	0.526	0	0.171
46.2	0.480	0.399	0	0.122
54.2	0.865	0.0973	0	0.0376
58.3	0.986	0.0108	0	.00307
Second Run				
0	0	0.833	0	0.167
10.8	0.0687	0.772	0	0.160
21.9	0.165	0.670	0	0.138
32.0	0.203	0.656	0	0.141
41.3	0.273	0.583	0	0.144
50.9	0.676	0.260	0	0.0636
57.0	0.981	0.0137	0	0.00569

Table B-30: PRSV-HV-UNIQUAC predicted concentrations for Toluene/Acetaminophen/Phenanthrene/CO₂ system at 25 °C

Predicted Values				
	CO ₂	Toluene	Phenanthrene	Acetaminophen
Pressure (bar)	x1	x2	x3	x4
1	0.00878	0.758	0.233	8.65E-05
3	0.0224	0.745	0.233	8.64E-05
5	0.0455	0.722	0.232	8.63E-05
10	0.0927	0.677	0.230	8.61E-05
20	0.193	0.585	0.222	8.53E-05
30	0.304	0.489	0.207	8.41E-05
40	0.437	0.385	0.178	8.20E-05
45	0.524	0.324	0.152	7.99E-05
50	0.673	0.231	0.0960	7.34E-05
60	0.988	0.00627	0.00569	2.47E-05

Table B-31: UNIQUAC interaction parameter matrix for Toluene/Acetaminophen/Phenanthrene/CO₂

u _{ij}	CO ₂	Toluene	Phenanthrene	Acetaminophen
CO ₂	0	179.18	349.7385822	752.7798227
Toluene	604.546	0	128.3495855	835.6408515
Phenanthrene	756.167	-72.434	0	818.3431792
Acetaminophen	1152.01	-8.0611	65.87010824	0

Table B-32: Experimental Mole fractions and pressures for Acetone/Acetaminophen/Phenanthrene/CO₂ system at 25 °C

Predicted Values				
	CO ₂	Acetone	Acetaminophen	Phenanthrene
Pressure (bar)	x1	x2	x3	x4
12.7	0.075	0.859	0.0156	0.0506
21.2	0.185	0.757	0.0113	0.0465
31.4	0.470	0.496	0	0.0325
40.1	0.609	0.376	0	0.0145
49.6	0.773	0.222	0	0.00472
58.5	0.962	0.036	0	0.00151

Table B-33: PRSV-HV-UNIQUAC predicted concentrations for Acetone/Acetaminophen/Phenanthrene/CO₂ system at 25 °C

Predicted Values				
	CO ₂	Acetone	Phenanthrene	Acetaminophen
Pressure (bar)	x1	x2	x3	x4
1	0.0138	0.802	0.178	0.00599
5	0.0886	0.741	0.166	0.00506
10	0.184	0.664	0.148	0.00405
20	0.380	0.512	0.105	0.00238
25	0.482	0.435	0.0815	0.00169
30	0.583	0.357	0.0591	0.00112
40	0.763	0.210	0.0269	0.000382
50	0.897	0.0916	0.0116	0.000104
60	0.987	0.00736	0.00535	2.68E-05

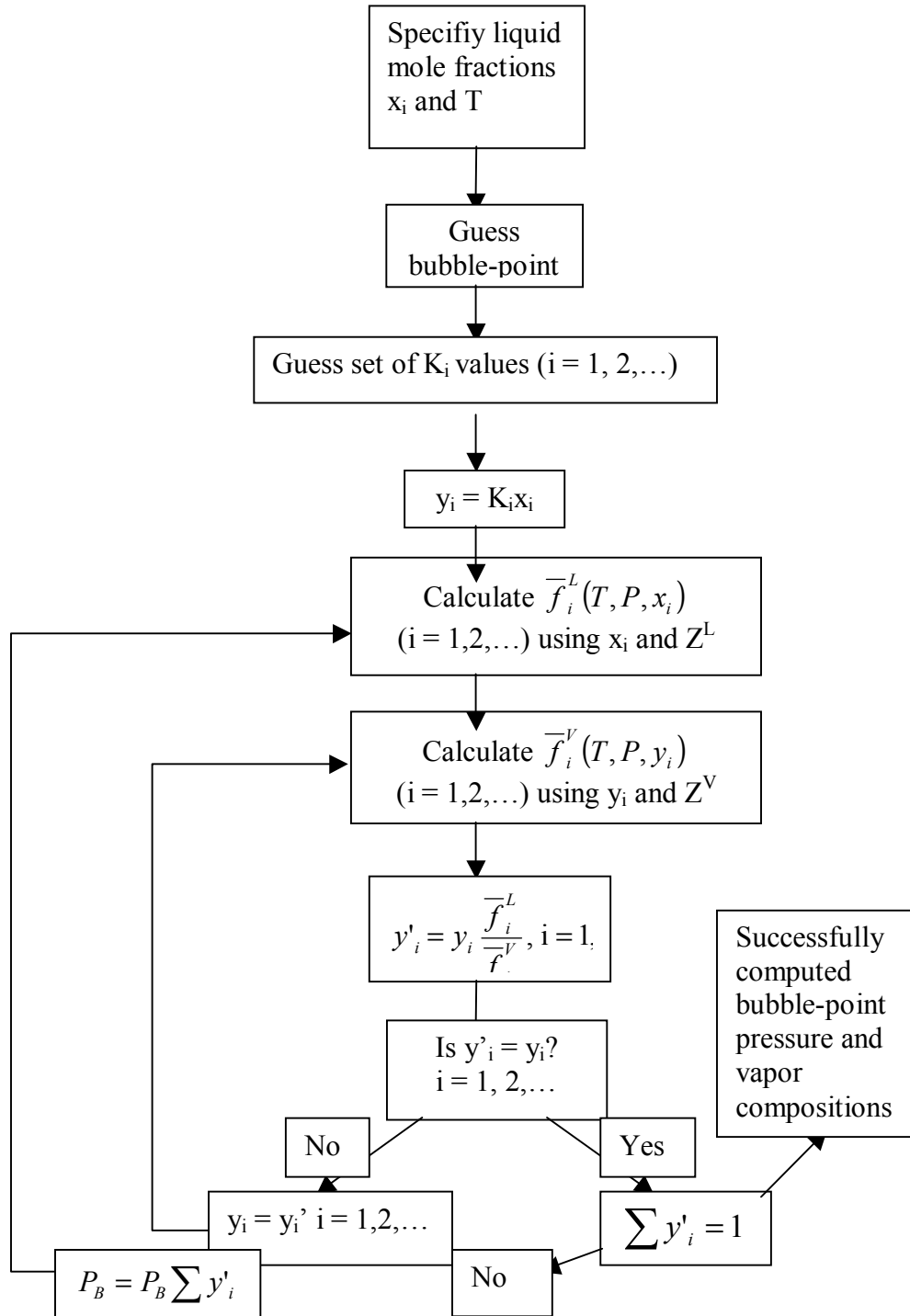
Table B-34: UNIQUAC interaction parameter matrix for Acetone/Acetaminophen/Phenanthrene/CO₂

u _{ij}	CO ₂	Acetone	Phenanthrene	Acetaminophen
CO ₂	0	-176.388	271.9483225	724.865037
Acetone	369.997817	0	-217.787146	30.7580393
Phenanthrene	560.475088	332.3661	0	818.343179
Acetaminophen	899.926834	259.539	65.87010824	0

APPENDIX C

BUBBLE POINT CALCULATION FLOW CHART

Figure C-1: Bubble Point Calculation Flow Sheet



REFERENCES

- Abdulkadirova, K. S., Khokhlachev, S.P. (1997). "Prediction of phase equilibria in hydrocarbon+near-critical solvent systems." Fluid Phase Equilibria **140**: 73-85.
- Abrams, D. S., Prausnitz, J. M. (1975). "Statistical thermodynamics of liquid mixtures. New expression for the excess Gibbs energy of partly or completely miscible systems." AIChE Journal **21**(1): 116-128.
- Acree, W., Abraham, M. (2001). "Solubility predictions for crystalline nonelectrolyte solutes dissolved in organic solvents based upon the Abraham general solvation model." Canadian Journal of Chemistry **79**: 1466-1476.
- Adrian, T., Maurer, G. (1997). "Solubility of Carbon Dioxide in Acetone and Propionic Acid at Temperatures between 298 K and 333 K." Journal Chemical and Engineering Data **42**: 668-672.
- Adrian, T., Oprescu, S., Maurer, G. (1997). "Experimental investigation of the multiphase high-pressure equilibria of carbon dioxide-water-(1-propanol)." Fluid Phase Equilibria **132**: 187-203.
- Amy, T., Eckert, C (2000). "Commentary on Supercritical Fluids: Research and Applications." Industrial and Engineering Chemistry Research **39**(12): 4442-4444.
- AP (2004). List of the Fortune 500. USA Today.
- Artal, M., et al (2001). "Representation for binary mixtures of n-alcohols + sub and supercritical CO₂ by a group-contribution method." Fluid Phase Equilibria **178**: 119-130.
- Beckman, E. (2004). "Supercritical and near-critical CO₂ in green chemical synthesis and processing." Journal of Supercritical Fluids **28**: 121-191.
- Bertucco, A., Lora, M., Kikic, I. (1998). "Fractional crystallization by gas antisolvent technique: theory and experiments." AIChE Journal **44**: 2149-2158.
- Blas, F., Galindo, A. (2002). "Study of the high pressure phase behaviour of CO₂ + n-alkane mixtures using the SAFT-VR approach with transferable parameters." Fluid Phase Equilibria **194-197**: 501-509.
- Bozan, B., Temelli, F. (2002). "Supercritical CO₂ extraction of flaxseed." Journal of the American Oil Chemists' Society **79**(3): 231-235.
- Bravi, M., Bubbico, R., Manna, F., Verdone, N. (2002). "Process optimisation in sunflower oil extraction by supercritical CO₂." Chemical Engineering Science **57**(14): 2753-2764.

- Bungert, B., Sadowski, G., Arlt, W. (1998). "Separations and Material Processing in Solutions with Dense Gases." Industrial and Engineering Chemistry Research **37**: 3208-3220.
- Burke, J. (1984). Solubility Parameters: Theory and Application. AIC Book and Paper Group Annual. C. Jensen, Book and Paper Group. **3**: 13-58.
- Chiehming, C., Kou-Lung, C., Chang-Yih, D. (1998). "A new apparatus for the determination of P-x-y diagrams and Henry's constants in high pressure alcohols with critical carbon dioxide." Journal of Supercritical Fluids **12**: 223-237.
- Christov, M., Dohrn, R. (2002). "High-pressure fluid phase equilibria Experimental methods and systems investigated (1994-1999)." Fluid Phase Equilibria **202**: 153-218.
- Cygnarowicz-Provost, M. (1996). "Design and Economic Analysis of Supercritical Fluid Extraction Processes." Supercritical Fluid Technology in Oil and Lipid Chemistry: 155-179.
- da Rocha, S., de Oliveira, J., d' Avila, S. (1996). "A three-phase ternary model for CO₂-solid-liquid equilibrium at moderate pressures." Journal of Supercritical Fluids **9**: 1-5.
- Day, C.-Y., Chang, Ch., Chen, Ch.-Y. (1996/1999). "Phase Equilibrium of Ethanol + CO₂ and Acetone + CO₂ at Elevated Pressures." Journal Chemical and Engineering Data **41/44**: 839-843/365.
- Diefenbacher, A., Turk M. (2002). "Phase equilibria of organic solid solutes and supercritical fluids with respect to the RESS process." JOURNAL OF SUPERCRITICAL FLUIDS **22**(3): 175-184.
- Dixon, D., Johnston, K. (1991). "Molecular thermodynamics of solubilities in gas antisolvent crystallization." AIChE Journal **37**: 1441-1449.
- Dostal, V., et al (2002). A supercritical CO₂ gas turbine power cycle for next-generation nuclear reactors. Proceedings of the International Conference on Nuclear Engineering, Arlington, VA, United States.
- Eckert, C., et al (2000). "Tuning Solvents for Sustainable Technology." Industrial and Engineering Chemistry Research **39**: 4615-4621.
- Elvassore, N., Striolo, A., Bertucco, A. (2002). "Thermodynamic modeling of high-pressure equilibria within the McMillan-Mayer framework." Fluid Phase Equilibria **194-197**: 587-598.
- Fusaro, F., Mazzotti, M (2004). "Gas Antisolvent Recrystallization of Paracetamol from Acetone Using Compressed Carbon Dioxide as Antisolvent." Crystal Growth and Design (Article): ASAP Article.

- Gani, R., Hytoft, G., Jakobsen, C. (1997). "Design and Analysis of Supercritical Extraction Processes." Applied Thermal Engineering **17**(8-10): 889-899.
- Geankoplis, C. J. (1993). Viscosity of Fluids. Transport Processes and Unit Operations. Englewood Cliffs, NJ, Prentice-Hall Inc.: 43-47.
- Granberg, R., Rasmussen, A. (1999). "Solubility of Paracetamol in Pure Solvents." Journal Chemical and Engineering Data **44**: 1391-1395.
- Hakuta, Y., Hayashi, H., Arai, K. (2003). "Fine particle formation using supercritical fluids." CURRENT OPINION IN SOLID STATE & MATERIALS SCIENCE **7**(4-5): 341-351.
- Hallet, J., Lu, J., Bush, D., Brown, J., Janak, M., Eckert, C., Liotta, C. (2003). Microscopically Probing the Tunable Solvent Properties of CO₂-Expanded Liquids (GXLs).
- Hauthal, W. (2001). "Advances with supercritical fluids [review]." Chemosphere **43**: 123-135.
- Hawthorne, S., et al (1993). "Preprints of Papers presented at the ACS National Meeting, American Chemical Society, Division of Environmental Chemistry." **33**(1): 331-334.
- Hines, A., and Maddox, R. (1985). Diffusion Coefficients. Mass Transfer. Upper Saddle River, NJ, Prentice Hall PTR: 27-38.
- Hong, L., Guo, J., Gao, Y., Yuan, W. (2000). "Precipitation of microparticulate organic pigment powders by a supercritical antisolvent process." Industrial and Engineering Chemistry Research **39**: 4882-4887.
- Huang, S., Radosz, M. (1990). "Phase behavior of reservoir fluids. II: Supercritical carbon dioxide and bitumen fractions." Fluid Phase Equilibria **60**(1-2): 81-98.
- Huron, M., Vidal, J. (1979). "New mixing rules in simple equations of state for representing vapor-liquid equilibria of strongly non-ideal mixtures." Fluid Phase Equilibria **3**(4): 255-271.
- Hwang, J., et al (1995). "Phase Behavior of CO₂/Crude Oil Mixtures in Supercritical Fluid Extraction System: Experimental Data and Modeling." Industrial and Engineering Chemistry Research **34**: 1280-1286.
- Ioannidis, S., Knox, D. (2001). "Vapor-liquid equilibria predictions at high pressures with the Huron-Vidal mixing rule." Fluid Phase Equilibria **187-188**: 1-14.
- Jensen, M. e. a. (2003). "Crystallisation of heavy hydrocarbons from three synthetic condensate gases at high pressure." Fluid Phase Equilibria **208**(1-2): 247-260.

- Jung, J., Perrut, M. (2001). "Particle design using supercritical fluids: Literature and patent survey." Journal of Supercritical Fluids **20**(3): 179-219.
- Kayrak, D., Akman, U., Hortacsu, O. (2003). "Micronization of Ibuprofen by RESS." Journal of Supercritical Fluids **26**: 17-31.
- Keshtkar, A., Jalali, F., Moshfeghian (1997). "Evaluation of vapor-liquid equilibrium of CO₂ binary systems using UNIQUAC-based Huron-Vidal mixing rules." Fluid Phase Equilibria **140**: 107-128.
- Kikic, I., Lora, M., Bertucco, A. (1997). "A Thermodynamic Analysis of Three-Phase Equilibria in Binary and Ternary Systems for Applications in Rapid Expansion of a Supercritical Solution (RESS), Particles from Gas-Saturated Solutions (PGSS), and Supercritical Antisolvent (SAS)." Industrial and Engineering Chemistry Research **36**: 5507-5515.
- Knudsen, K., Stenby, E., Fredenslund, A. (1993). "A comprehensive comparison of mixing rules for calculation of phase equilibria in complex systems." Fluid Phase Equilibria **82**: 361-368.
- Kordikowski, A., et al (1995). "Volume Expansions and Vapor-Liquid Equilibria of Binary Mixtures of a Variety of Polar Solvents and Certain Near-Critical Solvents." Journal of Supercritical Fluids **8**: 205-216.
- Kubatova, B., et al (2002). "Thermodynamic and kinetic models for the extraction of essential oil from savory and polycyclic aromatic hydrocarbons from soil with hot (subcritical) water and supercritical CO₂." Journal of Chromatography, A **975**(1): 175-188.
- Laube, D. (2001). "Limitations of CO₂ cleaning for semiconductor process tools." A2C2 **4**(2): 9-12.
- Laugier, S., Richon, D., Renon, H. (1994). "Ethylene + Olefin Binary Systems: Vapor-Liquid Equilibrium Experimental Data and Modeling." Journal Chemical and Engineering Data **39**: 388-391.
- Levitin, G., Myneni, S., Hess, D. (2004). "Post Plasma Etch Residue Removal Using CO₂-TMAHCO₃ Mixtures: Comparison of Single-Phase and Two-Phase Mixtures." Journal of Electrochemical Society **151**: G380-G386.
- Lin, C., Muhrer, G., Mazzotti, M. (2003). "Vapor-Liquid Mass Transfer during Gas Antisolvent Recrystallization: Modeling and Experiments." Industrial and Engineering Chemistry Research **42**: 2171-2182.

- Liu, G.-T., Nagahama, K. (1996). "Application of Rapid Expansion of Supercritical Solutions in the Crystallization Separation." Industrial and Engineering Chemistry Research **35**: 4626-4634.
- Liu, Z., Yang, G., Ge, L., Han, B. (2000). "Solubility of o- and p-Aminobenzoic Acids in Ethanol + Carbon Dioxide at 308.15 K to 318.15 K and 15 bar to 85 bar." Journal Chemical and Engineering Data **45**: 1179-1181.
- M. R. Jensen, e. a. (2003). "Crystallisation of heavy hydrocarbons from three synthetic condensate gases at high pressure." Fluid Phase Equilibria **208**: 247-260.
- Marr, R., Gamse, T. (2000). "Use of supercritical fluids for different processes including new developments-a review." Chemical Engineering and Processing **39**: 19-28.
- Marteau, P., et al (1996). "In situ determination of high pressure phase diagrams of methane-heavy hydrocarbon mixtures using an infrared absorption method." Fluid Phase Equilibria **119**: 213-230.
- Miura, K., Yamamura, K., Koizumi, M. (2003). "Apparatus for removal of oil utilizing supercritical fluid." Japan Kokai Tokkyo Koho: 6.
- Montero, G., Giorgio T., Schnelle Jr, K. (1996). "Scale-up and economic analysis for the design of supercritical fluid extraction equipment for remediation of soil." Environmental Progress **15**: 112-121.
- Muhrer, G., Lin, C., Mazzotti M. (2002). "Modeling the Gas Antisolvent Recrystallization Process." Industrial and Engineering Chemistry Research **41**: 3566-3579.
- Mukhopadhyay, M. (2003). "Partial molar volume reduction of solvent for solute crystallization using carbon dioxide as antisolvent." Journal of Supercritical Fluids **25**: 213-223.
- Mukhopadhyay, M., Dalvi, S. (2004). "Partial molar volume fraction of solvent in binary (CO₂-solvent) solution for solid solubility predictions." Journal of Supercritical Fluids **29**: 221-230.
- Mukhopadhyay M., J., N. (2003). "Supercritical carbon dioxide fractionation of vitamins E and A from vegetable sources." Indian Chemical Engineering **45**: 157-162.
- Myneni, S., Hess, D. (2002). "Fluorocarbon film and residue removal using supercritical CO₂ mixtures." Proceedings - Electrochemical Society **2002**(15(Enivronmental Issues with Materials and Processes for the Electronics and Semiconductor Industries): 180-189.
- Odabasi, A., Balaban, M. (2002). "Supercritical CO₂ extraction of sesame oil from raw seeds." Journal of Food Science and Technology **39**(5): 496-501.

- Orbey, H., Sandler, S. (1996). "A Comparison of Various Cubic Equation of State Mixing Rules for the Simultaneous Description of Excess Enthalpies and Vapor-Liquid Equilibria." Fluid Phase Equilibria **121**: 67-83.
- Patel, N., Teja, A. (1982). "A new cubic equation of state for fluids and fluid mixtures." Chemical Engineering Science **37**: 463-473.
- Pawar, R., et al (2003). Geologic Sequestration of CO₂ in a depleted oil reservoir. Abstracts of Papers, 226th ACS National Meeting, New York, NY, United States.
- Peng, D.-Y. a. R., D. B. (1976). "A New Two-Constant Equation of State." Industrial and Engineering Chemistry Fundamentals **15**: 59-64.
- Perrut, M. (2000). "Supercritical Fluid Applications: Industrial Developments and Economic Issues." Industrial and Engineering Chemistry Research **39**: 4531-4535.
- Pohler, H., Kiran, E. (1997). "Volumetric Properties of Carbon Dioxide + Acetone at High Pressures." Journal Chemical and Engineering Data **42**: 379-383.
- Prausnitz, J., Shair, F (1961). "Thermodynamic correlation of gas solubilities." AIChE Journal **7**: 682-687.
- Sala, S. (2004). "Molecular insight, through IR spectroscopy, on solvating phenomena occurring in CO₂-expanded solutions." ChemPhysChem **5**(2): 243-245.
- Sandler, S. I. (1999). Chapter 8: Phase Equilibrium in Mixtures. Chemical and Engineering Thermodynamics. New York, NY, John Wiley & Sons, Inc.: 478-629.
- Schroeder, C., et al (2001). "Progress in Mining and Oilfield Chemistry."
- Scurto, A., et. al. (2003). "Phase Behavior and Reliable Computation of High-Pressure Solid-Fluid Equilibrium with Cosolvents." Industrial and Engineering Chemistry Research **42**: 6464-6475.
- Shekunov, B. Y., Baldyga, J., York, P. (2001). "Particle formation by mixing with supercritical antisolvent at high Reynolds numbers." Chemical Engineering Science **56**: 2421-2433.
- Smith, C., Huse, G. (1998). "Equipment cost considerations and financial analysis of supercritical fluid processing." Supercritical Fluid Cleaning: 245-266.
- Spricigo, C., et al (2001). "Separation of nutmeg essential oil and dense CO₂ with a cellulose acetate reverse osmosis membrane." Journal of Membrane Science **188**(2): 173-179.

Spuller, M., Hess, D (2004). "CO₂-expanded liquids as alternatives to conventional solvents for resist and residue removal." Proceedings - Electrochemical Society **26** (**Cleaning Tehcnology in Semiconductor Device Manufacturing VIII**): 240-245.

Stryjek, R. a. V., J.H. (1986). "PRSV - An Improved Peng-Robinson Equation of State with New Mixing Rules for Strongly Nonideal Mixtures." Canadian Journal of Chemistry **64**: 334-340.

Subra, P., Jestin, P. (2000). "Screening Design of Experiment (DOE) Applied to Supercritical Antisolvent Process." Industrial and Engineering Chemistry Research **39**: 4178-4184.

Tai, C., Cheng, C-S. (1998). "Effect of CO₂ on Expansion and Supersaturation of Saturated Solutions." AIChE Journal **44**(4): 989-992.

Thiering, R., Dehghani, F., Foster, N. (2001). "Current issues relating to anti-solvent micronisation techniques and their extension to industrial scales." Journal of Supercritical Fluids **21**: 159-177.

Thomas, E., Eckert, C. (1984). "Prediction of Limiting Activity Coefficients by a Modified Separation of Cohesive Energy Density Model and UNIFAC." Industrial and Engineering Chemistry Process Design and Development **23**: 194-209.

van der Stegen, D. (1977). Removal of caffeine from coffee. Germany: 9.

Ventosa, N., Sala, S., Veciana, J. (2003). "DELOS process: a crystallization technique using compressed fluids. 1. Comparison to the GAS crystallization method." Journal of Supercritical Fluids **26**: 33-45.

Warwick, B., et al (2000). "Synthesis, Purification, and Micronization of Pharmaceuticals Using the Gas Antisolvent Technique." Industrial and Engineering Chemistry Research **39**: 4571-4579.

Weber, D., McGovern, W., Moses J. (1995). "Precision surface cleaning with supercritical carbon dioxide: Issues, experience, and prospects." Metal Finishing **93**(3): 22-26.

Weibel, G. L., Ober, C. K. (2002). "An overview of supercritical CO₂ applications in microelectronics processing." Microelectronics Engineering **65**: 145-152.

Wellington, S. L. (1982). Petroleum recovery from fields using carbon dioxide. Germany: 30.

Wendland, M., Hasse, H., Maurer, G. (1999). "Experimental Pressure-Temperature Data on Three- and Four-Phase Equilibria of Fluid, Hydrate, and Ice Phases in the System Carbon Dioxide-Water." Journal Chemical and Engineering Data **44**: 901-906.

West, K., et al (2001). " In Situ Formation of Alkylcarbonic Acids with CO₂." Journal of Physical Chemistry A **105**: 3947-3948.

Westrich, H., et al Sequestration of CO₂ in a Depleted Oil Reservoir: An Overview.
Sandia National Laboratories.

Zhang, X., et al (2002). "Determination of constant volume heat capacity of mixed supercritical fluids and study on the intermolecular interaction." Journal of Supercritical Fluids **24**: 193-201.

Zhi-Yu, Z., Ji-Chu, Y., Yi-Gui, L. (2000). "Prediction of phase equilibria for CO₂–C₂H₅OH–H₂O system using the SAFT equation of state." Fluid Phase Equilibria **169**: 1-18.